# 7

# HORN ANTENNAS

Horn antennas have a long history, traced in part in the collection of papers by Love [1] together with papers on every other horn topic. Horns have a wide variety of uses, from small-aperture antennas to feed reflectors to large-aperture antennas used by themselves as medium-gain antennas. Horns can be excited in any polarization or combination of polarizations. The purity of polarization possible and the unidirectional pattern make horns good laboratory standards and ideal reflector feeds. Horns also closely follow the characteristics predicted by simple theories.

Horns are analyzed using a variety of techniques. Barrow and Chu [2] analyzed a sectoral horn, flaring in only one plane, by solving the boundary value problem in the wedge. They expanded the fields in terms of Hankel functions in cylindrical coordinates. The fields form an equiphase surface over a cylindrical cap to which the Kirchhoff–Huygens equivalent current method [Eq. (2-23)] can be applied to compute the pattern. Similarly, Schorr and Beck [3] use spherical Hankel and Legendre functions to analyze conical horns. The integration surface consists of a spherical cap. Schelkunoff and Friis [4] use the mouth of the horn as the aperture and approximate the phase distribution as quadratic. Both aperture theories have the same valid pattern range. The method predicts patterns accurately in the area in front of the aperture. The error increases as the plane of the aperture is approached. The predicted pattern remains continuous and gives no indication of its increasing error. GTD methods [5] predict the pattern both in back and in front of the aperture while providing estimates of the error in the predictions. Most of the details needed for design can be obtained from the aperture theory. Only GTD predicts sidelobes accurately, since no assumption of zero fields outside the horn aperture is made.

Figure 7-1 shows the general horn geometry. The input waveguide can be either rectangular or circular (elliptical). $W$ is the width of a rectangular aperture, and $a$ is the radius of a circular aperture. The distance from the junction of the projected sides

*Modern Antenna Design, Second Edition*, By Thomas A. Milligan

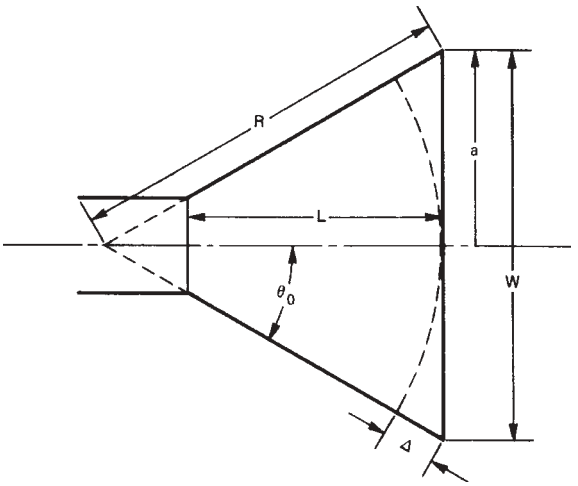


**FIGURE 7-1** General geometry of a horn.

to the aperture is the slant radius $R$. The distance along the centerline from the aperture to the waveguide is the axial length. We derive the aperture field amplitude from the input waveguide mode while the phase distribution is approximately quadratic across the aperture. We assume that the aperture fields radiate in spherical waves from the projected juncture of the sides, and the extra distance along the sides compared with the distance to the center of the aperture is given by

$$\begin{aligned}\Delta &= R - \sqrt{R^2 - a^2} \\ &= R\left(1 - \sqrt{1 - \frac{a^2}{R^2}}\right) \\ &\approx R\left[1 - \left(1 - \frac{a^2}{2R^2}\right)\right] = \frac{a^2}{2R} = \frac{W^2}{8R}\end{aligned}$$

We divide by wavelength to obtain the dimensionless constant $S$ of the quadratic phase distribution:

$$S = \frac{\Delta}{\lambda} = \frac{W^2}{8\lambda R} = \frac{a^2}{2\lambda R} \tag{7-1}$$

Since the semiflare angle $\theta_0$ of most practical horns is small, we use the quadratic phase error approximation.

## 7-1 RECTANGULAR HORN (PYRAMIDAL)

The rectangular horn flares out of a rectangular or square waveguide with flat metal walls. Figure 7-2 shows the horn geometry. The slant radiuses along the sides will be unequal, in general. The input waveguide dimensions are width $a$ and height $b$.

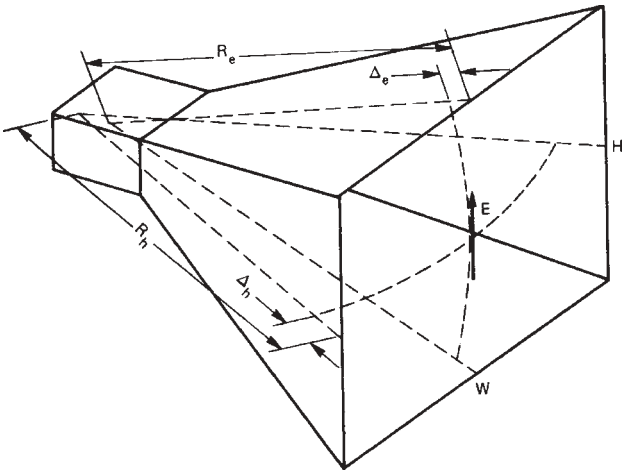


**FIGURE 7-2** Rectangular horn geometry.

The aperture has width W in the $H$-plane and height $H$ in the $E$-plane. Each aperture coordinate has its own quadratic phase distribution constant:

$$S_e = \frac{H^2}{8\lambda R_e} \qquad S_h = \frac{W^2}{8\lambda R_h} \tag{7-2}$$

The $TE_{10}$ mode of the lowest-order waveguide mode has the field distribution

$$E_y = E_0 \cos \frac{\pi x}{a}$$

Combining these ideas, the aperture electric field is approximated by

$$E_y = E_0 \cos \frac{\pi x}{W} \exp \left\{ -j2\pi \left[ S_e \left( \frac{2y}{H} \right)^2 + S_h \left( \frac{2x}{W} \right)^2 \right] \right\} \tag{7-3}$$

The ratio of the electric and magnetic fields approaches the impedance of free space for large apertures. In this case we use the Huygens source approximation and need only the electric field with Eq. (2-24) to find the pattern. Small-aperture horns require Eq. (2-23) with an arbitrary ratio of the magnetic and electric fields.

We compute the $E$-plane pattern by using a uniform aperture distribution and the $H$-plane pattern from a cosine distribution. Both have a quadratic phase error. Figures 7-3 and 7-4 plot the $E$- and $H$-plane universal patterns in $U$-space of the Taylor distribution with $S$ as a parameter. We can use them to determine the pattern of a general rectangular horn.

***Example*** Compute the pattern level at $\theta = 15^\circ$ in the $E$- and $H$-planes of a horn with the following measured dimensions:

*Aperture*: $W(H\text{-plane}) = 28.9\,\text{cm}$, $H(E\text{-plane}) = 21.3\,\text{cm}$
*Input waveguide*: width $a = 3.50\,\text{cm}$, height $b = 1.75\,\text{cm}$

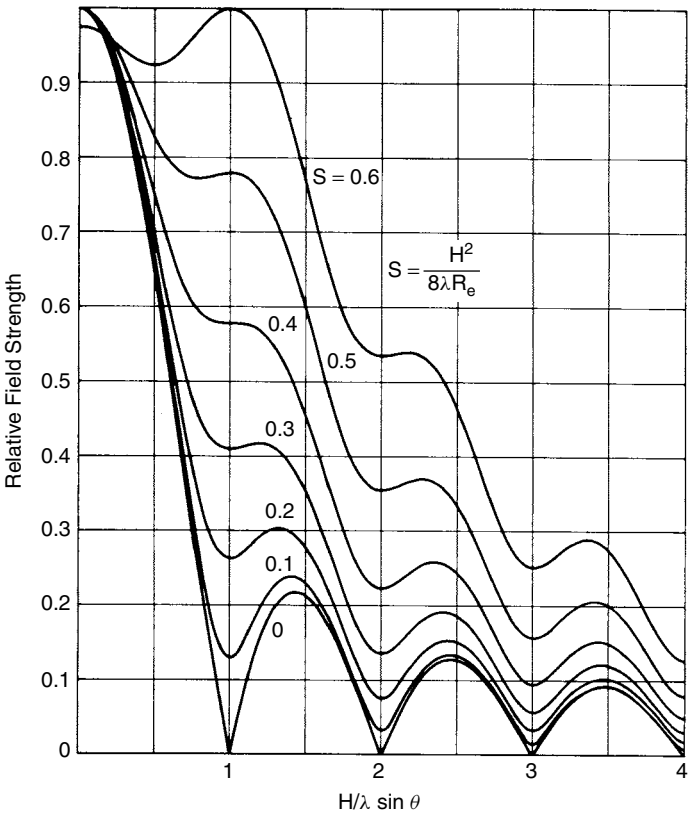


**FIGURE 7-3** $E$-plane universal pattern of a rectangular, $TE_{10}$ mode.

The slant distance from the aperture to the waveguide along the center of each plate of the flare was measured: $D_h = 44.8\,\text{cm}$ and $D_e = 44.1\,\text{cm}$. We calculate the slant radius from similar triangles:

$$\frac{R_h}{D_h} = \frac{W}{W - a} \qquad \frac{R_e}{D_e} = \frac{H}{H - b} \tag{7-4}$$

*Slant radius*: $R_h = 50.97\,\text{cm}$, $R_e = 48.05\,\text{cm}$

The frequency is 8 GHz ($\lambda = 3.75\,\text{cm}$). Using Eq. (7-2), we compute $S_h = 0.55$ and $S_e = 0.31$. We use Figures 7-3 and 7-4 to determine the universal pattern field intensity (voltage):

$$\frac{W}{\lambda}\sin\theta = 2.0 \qquad \frac{H}{\lambda}\sin\theta = 1.47$$

The fields from the figures are 0.27 ($H$-plane) and 0.36 ($E$-plane). We must include the obliquity factor of the Huygens source element pattern: $(1 + \cos\theta)/2$ to obtain the proper pattern level. At $\theta = 15^\circ$, the obliquity factor is 0.983. We calculate the pattern level in decibels from 20 times the logarithm of the product of the field intensity from

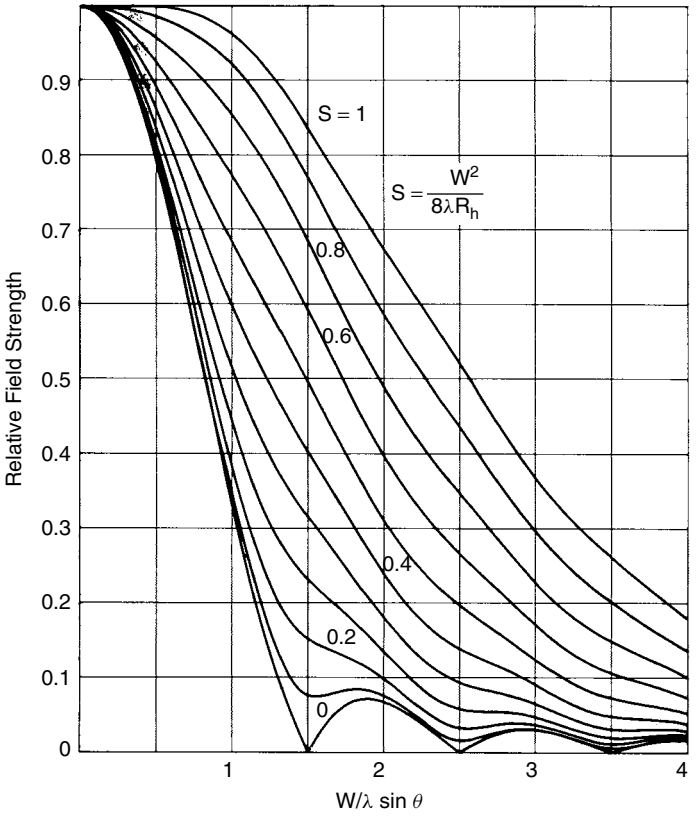


**FIGURE 7-4** $H$-plane universal pattern of a rectangular, $TE_{10}$ mode.

the figures and the obliquity factor:

$$H\text{-plane}: -11.5\,\text{dB} \qquad E\text{-plane}: -9\,\text{dB}$$

We can calculate gain of this horn by using aperture efficiencies:

$$H\text{-plane (cosine) (Table 4-1)}: \ 0.91\,\text{dB} \qquad E\text{-plane (uniform)}: \ 0\,\text{dB}$$

These values hold for all rectangular horns excited by the $TE_{10}$ mode. The quadratic phase distributions give us the phase error loss. From Table 4-42 we interpolate these losses:

$$S_h = 0.55 \text{ cosine distribution} \qquad \text{PEL} = 2.09\,\text{dB}$$
$$S_e = 0.31 \text{ uniform distribution} \qquad \text{PEL} = 1.50\,\text{dB}$$

The directivity is given by

$$\text{directivity} = 10\log\frac{4\pi WH}{\lambda^2} - \text{ATL}_h - \text{ATL}_e - \text{PEL}_h - \text{PEL}_e = 22.9\,\text{dB} \qquad (7\text{-}5)$$

The aperture efficiency is 35.5%, since $\text{ATL} + \text{PEL}_h + \text{PEL}_e = 4.5\,\text{dB}$.

We usually equate gain to directivity, since the wall losses are very small. Of course, for millimeter-wave horns we must include wall losses. Although we can use Table 4-42 along with the fixed-amplitude taper loss of 0.91 dB to determine the aperture efficiency of a rectangular horn, Schelkunoff and Friis [4] give the following closed-form equation for the directivity:

$$\text{directivity} = \frac{8R_hR_e}{WH}\{[C(u) - C(v)]^2 + [S(u) - S(v)]^2\}[C^2(z) + S^2(z)]$$

where

$$u = \frac{1}{\sqrt{2}}\left(\frac{\sqrt{\lambda R_h}}{W} + \frac{W}{\sqrt{\lambda R_h}}\right) \qquad v = \frac{1}{\sqrt{2}}\left(\frac{\sqrt{\lambda R_h}}{W} - \frac{W}{\sqrt{\lambda R_h}}\right) \qquad z = \frac{H}{\sqrt{2\lambda R_e}} \tag{7-6}$$

and

$$C(x) = \int_0^x \cos\frac{\pi t^2}{2}dt \qquad S(x) = \int_0^x \sin\frac{\pi t^2}{2}dt$$

are the Fresnel integrals. Closed-form expressions for these integrals are available [6].

### 7-1.1 Beamwidth

We can use Figures 7-3 and 7-4 to compute beamwidths. The 3-dB point corresponds to 0.707 and the 10-dB point to 0.316 on the graphs. Table 7-1 lists the 3- and 10-dB points (values of $U$) for different quadratic phase constants $S$ in the $H$-plane. Similarly, Table 7-2 lists the $E$-plane points. The tables are more convenient than the graphs. Because we remove the obliquity factor to get a universal pattern, we must modify the beamwidths found by using the tables. We find the beamwidth, but then we must add the obliquity factor to the beamwidth level. The beamwidth is found for

**TABLE 7-1 Rectangular-Horn $H$-Plane Beamwidth Points, $TE_{10}$ Mode**

| | $(W/\lambda)\sin\theta$ | | | $(W/\lambda)\sin\theta$ | |
|---|---|---|---|---|---|
| $S$ | 3 dB | 10 dB | $S$ | 3 dB | 10 dB |
| 0.00 | 0.5945 | 1.0194 | 0.52 | 0.8070 | 1.8062 |
| 0.04 | 0.5952 | 1.0220 | 0.56 | 0.8656 | 1.8947 |
| 0.08 | 0.5976 | 1.0301 | 0.60 | 0.9401 | 1.9861 |
| 0.12 | 0.6010 | 1.0442 | 0.64 | 1.0317 | 2.0872 |
| 0.16 | 0.6073 | 1.0652 | 0.68 | 1.1365 | 2.2047 |
| 0.20 | 0.6150 | 1.0949 | 0.72 | 1.2445 | 2.3418 |
| 0.24 | 0.6248 | 1.1358 | 0.76 | 1.3473 | 2.4876 |
| 0.28 | 0.6372 | 1.1921 | 0.80 | 1.4425 | 2.6246 |
| 0.32 | 0.6526 | 1.2700 | 0.84 | 1.5320 | 2.7476 |
| 0.36 | 0.6716 | 1.3742 | 0.88 | 1.6191 | 2.8618 |
| 0.40 | 0.6951 | 1.4959 | 0.92 | 1.7071 | 2.9744 |
| 0.44 | 0.7243 | 1.6123 | 0.96 | 1.7991 | 3.0924 |
| 0.48 | 0.7609 | 1.7143 | 1.00 | 1.8970 | 3.2208 |

**TABLE 7-2 Rectangular-Horn *E*-Plane Beamwidth Points, $TE_{10}$ Mode**

| | $(H/\lambda)\sin\theta$ | | | $(H/\lambda)\sin\theta$ | |
|---|---|---|---|---|---|
| $S$ | 3 dB | 10 dB | $S$ | 3 dB | 10 dB |
| 0.00 | 0.4430 | 0.7380 | 0.24 | 0.4676 | 1.4592 |
| 0.04 | 0.4435 | 0.7405 | 0.28 | 0.4793 | 1.5416 |
| 0.08 | 0.4452 | 0.7484 | 0.32 | 0.4956 | 1.6034 |
| 0.12 | 0.4482 | 0.7631 | 0.36 | 0.5193 | 1.6605 |
| 0.16 | 0.4527 | 0.7879 | 0.40 | 0.5565 | 1.7214 |
| 0.20 | 0.4590 | 0.8326 | 0.44 | 0.6281 | 1.8004 |

a lower pattern level than specified. Since the beamwidth levels are close, we use a relation by Kelleher [7, p. 12–5] with good results:

$$\frac{\text{BW}_2}{\text{BW}_1} = \sqrt{\frac{\text{level}_2(\text{dB})}{\text{level}_1(\text{dB})}} \tag{7-7}$$

***Example*** Compute 3- and 10-dB beamwidths for the horn in the preceding example. We have $S_h = 0.55$ and $S_e = 0.31$. From Tables 7-1 and 7-2,

$$\frac{W}{\lambda}\sin\theta_{h3} = 0.851 \qquad \frac{H}{\lambda}\sin\theta_{e3} = 0.4915$$

$$\frac{W}{\lambda}\sin\theta_{h10} = 1.8726 \qquad \frac{H}{\lambda}\sin\theta_{e10} = 1.588$$

$$\frac{W}{\lambda} = \frac{28.9}{3.75} = 7.707 \qquad \frac{H}{\lambda} = \frac{21.3}{3.75} = 5.68$$

$$\theta_{h3} = 6.34 \qquad \theta_{h10} = 14.06 \qquad \theta_{e3} = 4.96 \qquad \theta_{e10} = 16.24$$

We consider the obliquity factor, $(1 + \cos\theta)/2$, at these angles, and apply Eq. (7-7) to reduce the beamwidths found.

$$\text{BW}_{h3} = 12.68^\circ \text{at } 3.03\,\text{dB} \qquad \text{BW}_{h3}x = 12.62^\circ \text{at } 3.01\,\text{dB}$$

$$\text{BW}_{e3} = 9.92^\circ \text{at } 3.02\,\text{dB} \qquad \text{BW}_{e3} = 9.89^\circ \text{at } 3.01\,\text{dB}$$

$$\text{BW}_{h10} = 28.12^\circ \text{at } 10.13\,\text{dB} \qquad \text{BW}_{h10} = 27.94^\circ \text{at } 10\,\text{dB}$$

$$\text{BW}_{e10} = 32.48^\circ \text{at } 10.18\,\text{dB} \qquad \text{BW}_{10} = 32.2^\circ \text{at } 10\,\text{dB}$$

Including the obliquity factor has a very small effect on the results, but the effect increases with larger beamwidths (smaller apertures).

Aperture theory fails for small horns because the beam is determined more by edge diffraction than the aperture fields. Empirical data were collected and reduced to simple formulas for small rectangular horns based on aperture size only [8, p. 46–22]:

$$\text{BW}_{10e} = 88^\circ\frac{\lambda}{H} \quad \text{and} \quad \text{BW}_{10h} = 31^\circ + 79^\circ\frac{\lambda}{W}$$

### 7-1.2 Optimum Rectangular Horn

A rectangular horn has extra parameters, which we can use to design various optimum horns. Given a desired gain, we can design any number of horns with the same gain. Any optimum design depends on the requirements. Without any particular requirements, we will pick an antenna with equal $E$- and $H$-plane 3-dB beamwidths [9], but even this does not determine the design totally.

If we pick a constant slant radius and vary the aperture width, the gain increases with increasing aperture width, but the quadratic phase error loss increases faster and produces a maximum point. The maximum occurs in the two planes at approximately constant phase deviations independent of the slant radius:

$$S_h = 0.40 \qquad S_e = 0.26 \tag{7-8}$$

At these points we read the 3-dB points from Tables 7-1 and 7-2:

$$\frac{W}{\lambda}\sin\theta = 0.6951 \qquad \frac{H}{\lambda}\sin\theta = 0.4735$$

On dividing these equations to eliminate the constant $\sin\theta$ in the two planes, we derive the ratio of width to height to give a constant 3-dB beamwidth in the two planes for this optimum point:

$$\frac{H}{W} = 0.68 \tag{7-9}$$

The ratio depends on the beamwidth level. For 10-dB beamwidths,

$$\frac{H}{W} = 1.00 \tag{7-10}$$

These values of $S$ determine the efficiency of the optimum horn. We read the PEL of the quadratic phase distribution from Table 4-42 by using a cosine distribution for the $H$-plane and a uniform distribution for the $E$-plane. The $H$-plane distribution has an ATL of 0.91 dB.

$$\text{PEL}_h = 1.14\,\text{dB} \qquad \text{PEL}_e = 1.05\,\text{dB} \qquad \text{ATL} = 0.91\,\text{dB}$$

or an efficiency of 49%:

$$\text{gain} = \frac{4\pi HW}{\lambda^2}0.49$$

We solve for $H$ and $W$ for a given gain, since we know the ratio between them [Eq. (7-9)]:

$$\frac{W}{\lambda} = \sqrt{\frac{\text{gain}}{4\pi(0.68)(0.49)}} \qquad \frac{H}{\lambda} = \sqrt{\frac{\text{gain}(0.68)}{4\pi(0.49)}}$$

$$\frac{W}{\lambda} = 0.489\sqrt{\text{gain}} \qquad \frac{H}{\lambda} = 0.332\sqrt{\text{gain}} \tag{7-11}$$

We combine Eqs. (7-8) and (7-11) to calculate slant radiuses:

$$\frac{R_h}{\lambda} = 0.0746 \cdot \text{gain} \qquad \frac{R_e}{\lambda} = 0.0531 \cdot \text{gain} \tag{7-12a, b}$$

If, given gain, we use Eqs. (7-11) and (7-12) to design a horn, the dimensions will not be practical with an arbitrary input waveguide. The axial lengths from the waveguide to the aperture must be equal in the $E$- and $H$-planes, so the horn will meet the waveguide in a single plane. Given waveguide dimensions $a$ and $b$, the axial lengths are

$$L_h = \frac{W-a}{W}\sqrt{R_h^2 - \frac{W^2}{4}} \qquad L_e = \frac{H-a}{H}\sqrt{R_e^2 - \frac{H^2}{4}} \tag{7-13a, b}$$

We have a choice between retaining the $E$- or $H$-plane slant radius given by Eq. (7-12) and forcing the other radius to give the same axial length. The primary factor affecting gain is the aperture dimensions, which we retain from Eq. (7-11). The slant radius is secondary. We retain the $H$-plane radius calculated from Eq. (7-12) and modify the $E$-plane radius. Modifying the $H$-plane radius would give us a second optimum design:

$$R_e = \frac{H}{H-b}\sqrt{L^2 + \frac{(H-b)^2}{4}} \tag{7-14}$$

To obtain the proper gain, we must iterate, since we cannot use both Eq. (7-12). Design the horn by using Eqs. (7-11), (7-12$a$), (7-13$a$), and (7-14). Calculate the gain from the dimensions and obtain a new design gain from

$$G_{d,\text{new}} = \frac{G_{\text{required}} G_{d,\text{old}}}{G_{\text{actual}}} \tag{7-15}$$

where $G_{\text{required}}$ is the required gain, $G_{\text{actual}}$ is the actual gain, and $G_{d,\text{old}}$ is the old design gain.

***Example*** Design a horn fed from WR-90 waveguide to have 22 dB of gain at 10 GHz.

The waveguide dimensions are 2.286 cm × 1.016 cm (0.9 in. × 0.4 in.) and $G_{\text{req}} = G_d = 10^{22/10} = 158.5$.

On substituting in Eq. (7-11), we calculate aperture dimensions: $W = 18.47$ cm and $H = 12.54$ cm. From Eqs. (7-12$a$) and (7-13$a$), $R_h = 35.47$ cm and $L = 30.01$ cm. To get the same axial length in the $E$-plane [Eq. (7-14)], $R_e = 33.25$ cm. We now calculate gain and compare it with the gain required. The amplitude taper loss and phase error loss in the $H$-plane remain constant, since $S_h$ is fixed.

$$\text{ATL} = 0.91\,\text{dB} \qquad \text{PEL}_h = 1.14\,\text{dB} \quad \text{at} \quad S_h = 0.40$$

Calculate $S_e$:

$$S_e = \frac{H^2}{8\lambda R_e} = 0.197 \qquad \text{PEL}_e = 0.60\,\text{dB} \quad \text{(Table 4-42)}$$

$$G_{\text{actual}}(\text{dB}) = 10\log\frac{4\pi HW}{\lambda^2} - \text{ATL} - \text{PEL}_h - \text{PEL}_e = 22.45\,\text{dB}$$

$$= 175.8$$

We must pick a new design gain [Eq. (7-15)]:

$$G_{d,\text{new}} = \frac{158.5(158.5)}{175.8} = 142.9$$

A second iteration with this gain gives the following dimensions:

$$W = 17.54\,\text{cm} \qquad H = 11.91\,\text{cm} \qquad L = 26.75\,\text{cm} \qquad R_h = 31.98\,\text{cm}$$

$$R_e = 29.84\,\text{cm} \qquad S_e = 0.198 \qquad \text{PEL}_e = 0.60$$

$$\text{gain} = 10\log\frac{4\pi HW}{\lambda^2} - 0.91 - 1.14 - 0.60 = 22.00\,\text{dB}$$

We obtain the gain desired, but the 3-dB beamwidths are only approximately equal: $H$-plane: 13.66°, $E$-plane: 13.28°.

Scales 7-1 to 7-3 provide the dimensions of the optimum rectangular horn for a given gain. During their generation, a waveguide with a 2 : 1 aspect was used, but they are close to the proper values for nearby aspects. They design horns to within 0.1 dB. These scales produce short rapidly flaring horns for low-gain antennas. In these cases it is better to deviate from the optimum design that gives the lightest horn for a given gain and design a horn with a small value of $S$. Scales 7-4 to 7-6 give designs for $S = 0.1$ to be used for low-gain designs.

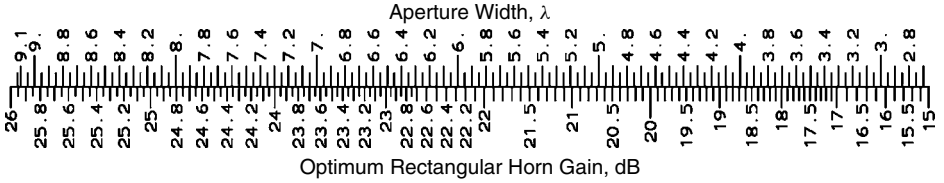


**SCALE 7-1** Aperture width of an optimum pyramidal horn for a 2 : 1-aspect waveguide.

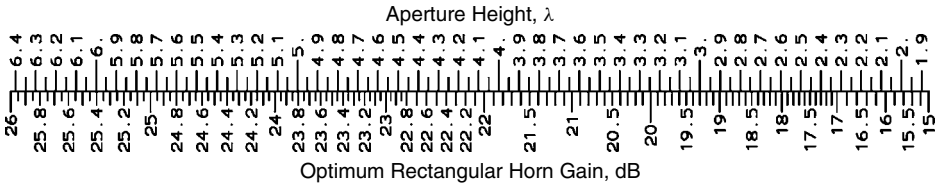


**SCALE 7-2** Aperture height of an optimum pyramidal horn for a 2 : 1-aspect waveguide.

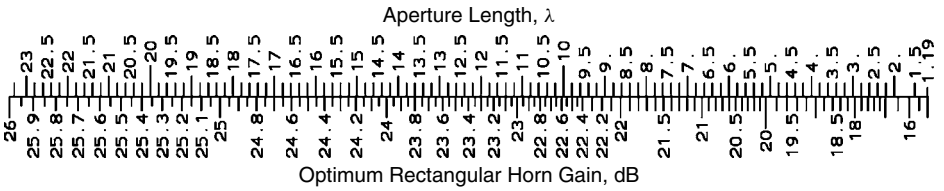


**SCALE 7-3** Axial length of an optimum pyramidal horn for a 2 : 1-aspect waveguide.

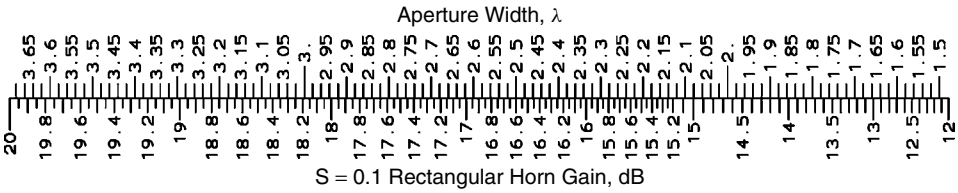


**SCALE 7-4** Aperture width of a pyramidal horn with $S = 0.1$ connected to a 2 : 1 waveguide.

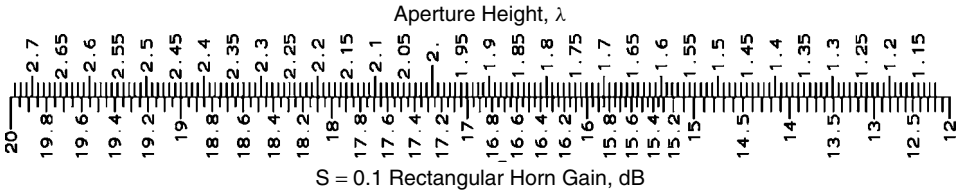


**SCALE 7-5** Aperture height of a pyramidal horn with $S = 0.1$ connected to a 2 : 1 waveguide.

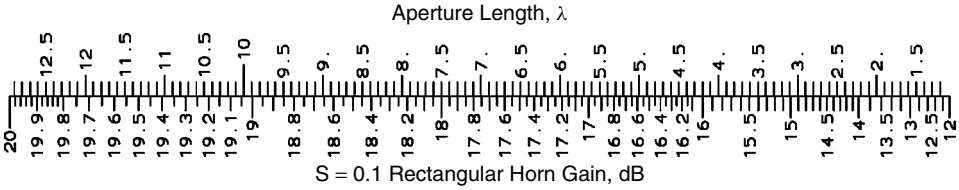


**SCALE 7-6** Axial length of a pyramidal horn with $S = 0.1$ connected to a 2 : 1 waveguide.

### 7-1.3 Designing to Given Beamwidths

The beamwidths in the two planes of a rectangular horn can be designed independently. The axial lengths in the two planes must be equal if the design is to be realizable, but the aperture width and height can be adjusted to give the desired beamwidths. We pick $S$ in one plane and then vary $S$ in the other plane to produce the required beamwidth and the same axial length as in the first plane. Since the first $S$ is arbitrary, the design is not unique, but in only a limited range of $S$ will designs be realizable.

***Example*** Design a rectangular horn for the following 10-dB beamwidths: 30° $H$-plane and 70° $E$-plane at 7 GHz using a 3.5-cm × 1.75-cm waveguide.

Since the $H$-plane has the narrower beamwidth and therefore the wider aperture, we use it to determine length. Pick $S_h = 0.20$ (an arbitrary choice). The obliquity factor at 15° is 0.15 dB. When using Table 7-1 we must design for wider than a 30° beamwidth to compensate for the obliquity factor:

$$\mathrm{BW}_d = \sqrt{\frac{10.15}{10}}(30^\circ) = 30.22^\circ$$

The horn width to provide that beamwidth is

$$\frac{W}{\lambda} = \frac{1.0949}{\sin(\mathrm{BW}_d/2)} = 4.200$$

$$W = 18.00\,\text{cm at } 7\,\text{GHz} \qquad R_h = 47.25 \quad \text{[Eq. (7.2)]}$$

Use Eq. (7-13*a*) to determine the axial length: $L_h = L = 37.36\,\text{cm}$. Because the $E$-plane beamwidth is wider than the $H$-plane beamwidth, the $E$-plane aperture will be smaller. We try a smaller value of $S_e$ than $S_h$ for our initial guess: $S_e = 0.04$. The obliquity factor at 35° adds 0.82 dB to the pattern loss and requires a larger design beamwidth.

$$\text{BW}_d = \sqrt{\frac{10.82}{10}}70^\circ = 72.82^\circ$$

$$\frac{H}{\lambda} = \frac{0.7405}{\sin(\text{BW}_d/2)} = 1.248 \quad \text{(Table 7-2)} \qquad H = 5.246$$

We use Eqs. (7-2) and (7-13*b*) to calculate slant radius and axial length: $R_e = 20.84\,\text{cm}$ and $L_e = 13.90\,\text{cm}$. The axial lengths in the two planes do not match, so we pick a smaller $S_e$ because the $E$-plane is shorter than the $H$-plane beamwidth. At $S_e = 0.02$, $H = 5.337\,\text{cm}$, $R_e = 41.54\,\text{cm}$, and $L_e = 27.86\,\text{cm}$. $L_e$ has doubled when $S_e$ changes from 0.04 to 0.02, but $H$ changes by only 0.01 cm. We change our method and pick $H = 5.33\,\text{cm}$ and force $R_e$ to give the same axial length as the $H$-plane: $R_e = 55.69\,\text{cm}$ [from Eq. (7-14)] or $S_e = 0.0149$.

### 7-1.4 Phase Center

We define the phase center as the point from which it appears that an antenna radiates spherical waves. Measurements show that the phase center is seldom a unique point in a plane, but depends on the pattern angle. The $E$- and $H$-plane phase centers will also be unequal in general. Usually, they are extremes, and the axial position varies elliptically between the planes. Even with the phase-center location fuzzy, it is a useful point. We place the phase center of a feed at the focus of a parabolic reflector to minimize the reflector aperture phase error loss.

An aperture with a quadratic phase distribution appears to be radiating from a point behind the aperture. Without quadratic phase error ($S = 0$), the phase center is located at the aperture plane. Increasing $S$ moves the phase center toward the apex of the horn. Muehldorf [10] has calculated the phase-center location as a function of $S$, and Table 7-3 summarizes his results. The phase center located inside the aperture is given as a ratio of the slant length.

**TABLE 7-3 Phase-Center Axial Location of a Rectangular Horn ($TE_{10}$ Mode) Behind the Aperture as a Ratio of the Slant Radius**

| $S$ | $H$-Plane $L_{ph}/R_h$ | $E$-plane $L_{ph}/R_e$ | $S$ | $H$-plane $L_{ph}/R_h$ | $E$-plane $L_{ph}/R_e$ |
|---|---|---|---|---|---|
| 0.00 | 0.0 | 0.0 | 0.28 | 0.258 | 0.572 |
| 0.04 | 0.0054 | 0.011 | 0.32 | 0.334 | 0.755 |
| 0.08 | 0.022 | 0.045 | 0.36 | 0.418 | |
| 0.12 | 0.048 | 0.102 | 0.40 | 0.508 | |
| 0.16 | 0.086 | 0.182 | 0.44 | 0.605 | |
| 0.20 | 0.134 | 0.286 | 0.48 | 0.705 | |
| 0.24 | 0.191 | 0.416 | 0.52 | 0.808 | |

***Example*** Calculate the phase-center location for the beamwidth design example above.

$$S_h = 0.20 \qquad R_h = 47.25\,\text{cm}$$
$$S_e = 0.015 \qquad R_e = 55.69\,\text{cm}$$

From Table 7-3, we interpolate

$$H\text{-plane phase center} = 0.134(47.25\,\text{cm}) = 6.33\,\text{cm}$$
$$E\text{-plane phase center} = 0.004(55.69\,\text{cm}) = 0.22\,\text{cm}$$

The difference in the phase-center location in the two planes is $1.43\lambda$.

As in the example, antennas with widely differing beamwidths will have widely separated phase centers.

## 7-2 CIRCULAR-APERTURE HORN

With a circular-aperture horn, we lose independent control of the beamwidths in the principal planes. The circular waveguide can support any orientation of the electric field and thereby allows any polarization in the horn. We use the same aperture field method as with the rectangular horn and the waveguide mode determines the aperture amplitude. The cone of the horn projects to a point in the feed waveguide where we assume a point source radiating to the aperture. The aperture phase is approximately quadratic. The waveguide fields are given by

$$E_\rho = \frac{E_0}{\rho} J_1\left(\frac{x'_{11}\rho}{a}\right)\cos\phi_c$$
$$E_{\phi_c} = -\frac{E_0 x'_{11}}{a} J'_1\left(\frac{x'_{11}\rho}{a}\right)\sin\phi_c \tag{7-16}$$

where $J_1$ is the Bessel function, $\rho$ the radial component in the waveguide, $a$ the radius, and $\phi_c$ the cylindrical coordinate. $x'_{11}$ (1.841) is the first zero of $J'_1(x)$. Equation (7-16) has its maximum electric field directed along the $\phi_c = 0$ plane.

We add the quadratic phase factor to Eq. (7-16) and calculate the Fourier transform on the circular aperture to determine the far field. The direction of the electric field changes from point to point in the aperture. For a given direction ($\theta$, $\phi_c$) we must project the fields in the aperture onto the $\hat{\theta}$ and $\hat{\phi}$ directions before integrating over the aperture:

$$E_\theta = E_0 \int_0^{2\pi}\int_0^a \left[\frac{J_1(x'_{11}\rho/a)}{\rho}\cos\phi_c \frac{\hat{\theta}\bullet\hat{\rho}}{\cos\theta} - \frac{x'_{11}}{a} J'_1\left(\frac{x'_{11}\rho}{a}\right)\sin\phi_c \frac{\hat{\theta}\bullet\hat{\phi}_c}{\cos\theta}\right]$$
$$\times\, \rho \exp\left\{j\left[k\rho\sin\theta\cos(\phi-\phi_c) - 2\pi S\left(\frac{\rho}{a}\right)^2\right]\right\} d\rho\, d\phi_c \tag{7-17}$$

$$E_\phi = E_0 \int_0^{2\pi} \int_0^a \left[ \frac{J_1(x'_{11}\rho/a)}{\rho} \cos\phi_c \hat{\phi}\cdot\hat{\rho} - \frac{x'_{11}}{a} J'_1\left(\frac{x'_{11}\rho}{a}\right) \sin\phi_c \hat{\phi}\cdot\hat{\phi}_c \right]$$
$$\times \rho \exp\left\{ j\left[ k\rho\sin\theta\cos(\phi-\phi_c) - 2\pi S\left(\frac{\rho}{a}\right)^2 \right] \right\} d\rho\, d\phi_c \qquad (7\text{-}18)$$

$$\hat{\theta}\cdot\hat{\rho} = \cos\theta(\cos\phi\cos\phi_c + \sin\phi\sin\phi_c)$$
$$\hat{\theta}\cdot\hat{\phi}_c = \cos\theta(\sin\phi\cos\phi_c - \cos\phi\sin\phi_c)$$
$$\hat{\phi}\cdot\hat{\rho} = \cos\phi\sin\phi_c - \sin\phi\cos\phi_c$$
$$\hat{\phi}\cdot\hat{\phi}_c = \cos\phi\cos\phi_c + \sin\phi\sin\phi_c$$

By a suitable change of variables in the integrals, universal radiation patterns can be generated for the $E$-and $H$-planes (Figures 7-5 and 7-6). The equality of $S$ in the two planes ties the curves together. The axis is the $k$-space variable. We can calculate a few pattern points for a given horn with those curves if we remember to add the obliquity factor to the values taken from the curves.

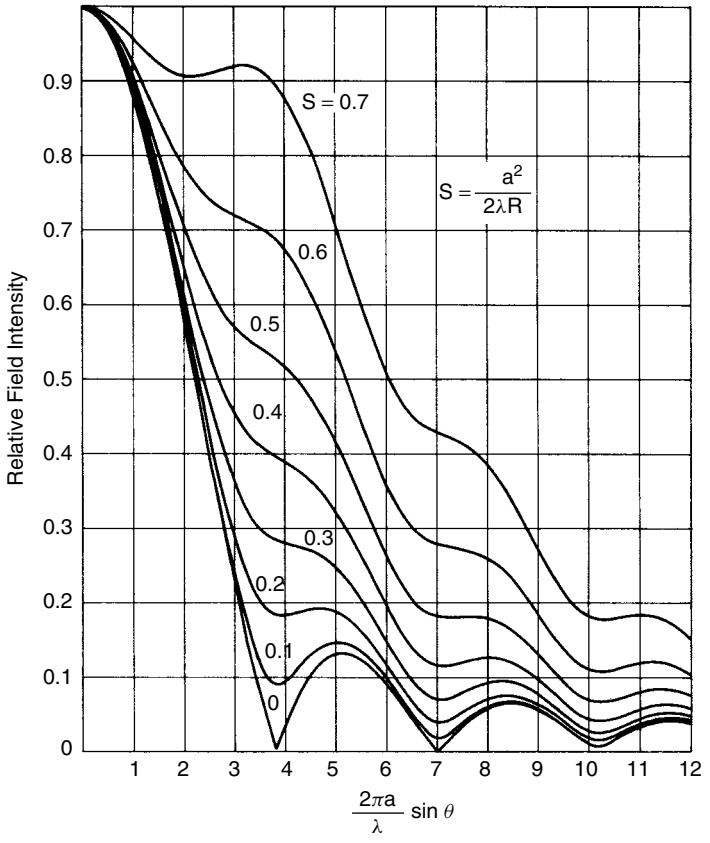


**FIGURE 7-5** $E$-plane universal pattern of a circular, $TE_{11}$ mode. (From T. Milligan, Universal patterns ease circular horn design, *Microwaves,* vol. 20, no. 3, March 1981, p. 84.)

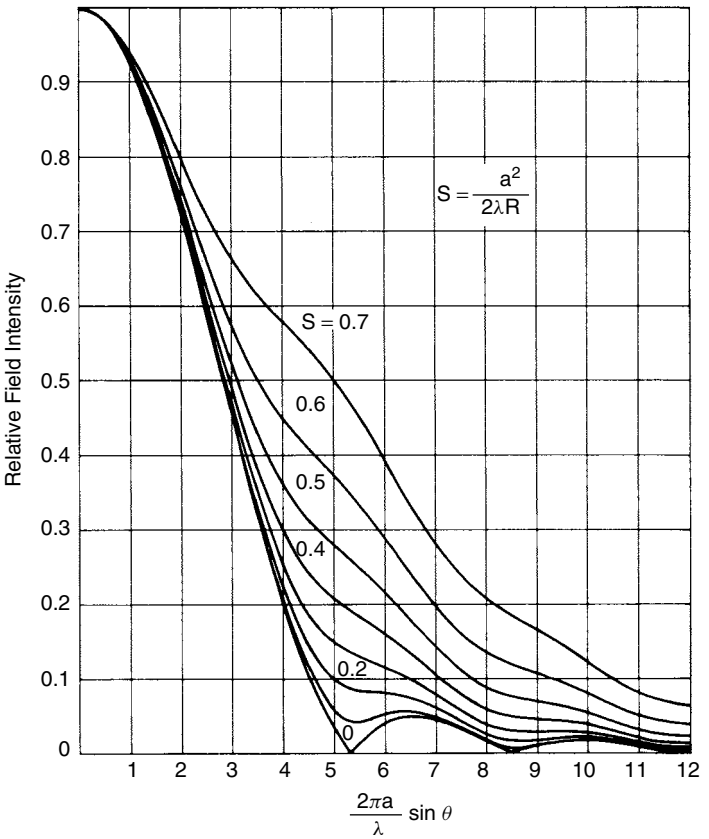


**FIGURE 7-6** $H$-plane universal pattern of a circular, $TE_{11}$ mode. (From T. Milligan, Universal patterns ease circular horn design, *Microwaves,* vol. 20, no. 3, March 1981, p. 84.)

***Example*** A horn has an aperture radius of 12 cm and a slant radius of 50 cm. Compute the pattern level at $\theta = 20^\circ$ at 5 GHz.

From Figures 7-5 and 7-6 we interpolate the pattern voltage level:

$$H\text{-plane level} = 0.18 \quad (-14.7\,\text{dB}) \qquad E\text{-plane level} = 0.22 \quad (-13.1\,\text{dB})$$

The obliquity factor is $20\log[(1 + \cos 20^\circ)/2] = -0.3\,\text{dB}$, and the plane level at 20° becomes

$$H\text{-plane level} = -15\,\text{dB} \qquad E\text{-plane level} = -13.4\,\text{dB}$$

### 7-2.1 Beamwidth

Table 7-4 lists the 3- and 10-dB points from Figures 7-5 and 7-6. We can use them to compute beamwidths from dimensions.

***Example*** Calculate 10-dB beamwidths of the horn in the example above. $S = 0.24$, $a = 12\,\text{cm}$, and $\lambda = 6\,\text{cm}$.

**TABLE 7-4 Circular-Horn Beamwidths, $TE_{11}$ Mode**

| | $(2\pi a/\lambda)\sin\theta$ | | | | |
|---|---|---|---|---|---|
| | 3 dB | | 10 dB | | ATL + PEL |
| $S$ | $E$-Plane | $H$-Plane | $E$-Plane | $H$-Plane | (dB) |
| 0.00 | 1.6163 | 2.0376 | 2.7314 | 3.5189 | 0.77 |
| 0.04 | 1.6175 | 2.0380 | 2.7368 | 3.5211 | 0.80 |
| 0.08 | 1.6212 | 2.0391 | 2.7536 | 3.5278 | 0.86 |
| 0.12 | 1.6273 | 2.0410 | 2.7835 | 3.5393 | 0.96 |
| 0.16 | 1.6364 | 2.0438 | 2.8296 | 3.5563 | 1.11 |
| 0.20 | 1.6486 | 2.0477 | 2.8982 | 3.5799 | 1.30 |
| 0.24 | 1.6647 | 2.0527 | 3.0024 | 3.6115 | 1.54 |
| 0.28 | 1.6855 | 2.0592 | 3.1757 | 3.6536 | 1.82 |
| 0.32 | 1.7123 | 2.0676 | 3.5720 | 3.7099 | 2.15 |
| 0.36 | 1.7471 | 2.0783 | 4.6423 | 3.7863 | 2.53 |
| 0.40 | 1.7930 | 2.0920 | 5.0492 | 3.8933 | 2.96 |
| 0.44 | 1.8552 | 2.1100 | 5.3139 | 4.0504 | 3.45 |
| 0.48 | 1.9441 | 2.1335 | 5.5375 | 4.2967 | 3.99 |
| 0.52 | 2.0823 | 2.1652 | 5.7558 | 4.6962 | 4.59 |
| 0.56 | 2.3435 | 2.2089 | 6.0012 | 5.2173 | 5.28 |
| 0.60 | 3.4329 | 2.2712 | 6.3500 | 5.6872 | 5.98 |
| 0.64 | 4.3656 | 2.3652 | 7.6968 | 6.0863 | 6.79 |
| 0.68 | 4.8119 | 2.5195 | 8.4389 | 6.4622 | 7.66 |
| 0.72 | 5.1826 | 2.8181 | 8.8519 | 6.8672 | 8.62 |

From Table 7-4 we read the $k$-space values at 10 dB:

$$H\text{-plane } k\text{-space} = \frac{2\pi a}{\lambda}\sin\theta_h = 3.6115$$

$$E\text{-plane } k\text{-space} = \frac{2\pi a}{\lambda}\sin\theta_e = 3.0024$$

$$\text{BW}_h = 2\sin^{-1}\frac{3.6115}{4\pi} = 33.40^\circ \qquad \text{BW}_e = 2\sin^{-1}\frac{3.0024}{4\pi} = 27.65^\circ$$

We must add the obliquity factor to the 10-dB universal pattern level:

$$\frac{1+\cos 16.7^\circ}{2}: \quad 0.18\,\text{dB} \qquad H\text{-plane}$$

$$\frac{1+\cos 13.8^\circ}{2}: \quad 0.13\,\text{dB} \qquad E\text{-plane}$$

$$\text{BW}_{h10} = \sqrt{\frac{10}{10.18}}33.40^\circ = 33.10^\circ \qquad \text{BW}_{e10} = \sqrt{\frac{10}{10.13}}27.65^\circ = 27.48^\circ$$

We can also use Table 7-4 to design a horn to a given beamwidth, but we can design to only one plane. Any number of horns can be designed to a given beamwidth, since $S$ is an independent parameter. Table 7-4 lists the combined amplitude taper loss and phase error loss as a function of $S$ for the circular horn. With this table we can easily estimate the gain of a given horn or design a horn to a given gain.

***Example*** Compute the gain of a horn with a 12-cm aperture radius and 50-cm slant radius at 5 GHz.

From the examples above we read $S = 0.24$ and $\lambda = 6\,\text{cm}$:

$$\begin{aligned}\text{gain} &= 20\log\frac{\pi D}{\lambda} - \text{GF} \qquad \text{where} \quad \text{GF} = \text{ATL} + \text{PEL (dB)} \\ &= 20\log\frac{24\pi}{6} - 1.54 = 20.4\,\text{dB}\end{aligned} \tag{7-19}$$

***Example*** Design a circular horn at 8 GHz with a gain of 22 dB.

The quadratic phase distribution constant $S$ is arbitrary. Pick $S = 0.20$. Rearrange Eq. (7-19) to find the diameter:

$$\begin{aligned}D &= \frac{\lambda}{\pi}\cdot 10^{(\text{gain}+\text{GF})/20} \\ &= \frac{3.75}{\pi}\cdot 10^{(22+1.30)/20} = 17.45\,\text{cm} \\ R &= \frac{D^2}{8\lambda S} = 50.77\,\text{cm}\end{aligned} \tag{7-20}$$

We can determine an optimum circular horn in the sense of minimizing the slant radius at a given gain. When we plot gain as a function of aperture radius for a fixed slant radius, we discover a broad region in which the gain peaks. By plotting a series of these lines with a voltage gain ordinate, we see that a single line corresponding to $S = 0.39$ can be drawn through the peaks. This is our optimum with GF = 2.85 dB (ATL + PEL).

***Example*** Design an optimum horn at 8 GHz with gain of 22 dB.

From Eq. (7-20),

$$D = \frac{3.75}{\pi}\cdot 10^{(22+2.85)/20} = 20.86\,\text{cm} \qquad R = \frac{D^2}{8\lambda S} = \frac{20.86^2}{8(3.75)(0.39)} = 37.2\,\text{cm}$$

The optimum is quite broad. A horn designed with $S = 0.38$ has a 0.07-cm-longer slant radius and a 0.25-cm-smaller aperture diameter.

### 7-2.2 Phase Center

The phase-center location behind the aperture plane is a function of $S$. Table 7-5 lists the phase-center location as a ratio of the slant radius. As $S$ increases, the phase center migrates toward the horn apex and the difference between the phase-center locations in the $E$- and $H$-planes increases.

***Example*** Use Table 7-5 to compute phase-center locations in the $E$- and $H$-planes for the circular horns of the preceding two examples.

$$\begin{aligned}R = 50.77\,\text{cm} \quad S = 0.20 \\ H\text{-plane phase center} = 0.117(50.77) = 5.94\,\text{cm} \\ E\text{-plane phase center} = 0.305(50.77) = 15.48\,\text{cm}\end{aligned}$$

**TABLE 7-5 Phase-Center Axial Location of a Circular-Waveguide Horn $TE_{11}$ Mode Behind the Aperture as a Ratio of the Slant Radius**

| $S$ | $H$-Plane $L_{ph}/R_h$ | $E$-Plane $L_{ph}/R_e$ | $S$ | $H$-Plane $L_{ph}/R_h$ | $E$-Plane $L_{ph}/R_e$ |
|---|---|---|---|---|---|
| 0.00 | 0.0 | 0.0 | 0.28 | 0.235 | 0.603 |
| 0.04 | 0.0046 | 0.012 | 0.32 | 0.310 | 0.782 |
| 0.08 | 0.018 | 0.048 | 0.36 | 0.397 | 0.801 |
| 0.12 | 0.042 | 0.109 | 0.40 | 0.496 | 0.809 |
| 0.16 | 0.075 | 0.194 | 0.44 | 0.604 | 0.836 |
| 0.20 | 0.117 | 0.305 | 0.48 | 0.715 | 0.872 |
| 0.24 | 0.171 | 0.416 | | | |

The phase centers differ by 2.5 wavelengths at 8 GHz. The optimum horn has the dimensions

$$R = 37.2\,\text{cm} \quad S = 0.39$$

$$H\text{-plane phase center} = 0.471(37.2) = 17.5\,\text{cm}$$

$$E\text{-plane phase center} = 0.807(37.2) = 30.0\,\text{cm}$$

The phase centers of the optimum horn differ by 3.3 wavelengths. The difference increases with increasing $S$.

## 7-3 CIRCULAR (CONICAL) CORRUGATED HORN

Normal smooth-wall horns present problems that can be eliminated by corrugating the walls. Many applications require dual linear or circular polarizations. The horn aperture must be square or circular and the beamwidths in the two planes are unequal. When the smooth-wall horn feeds a reflector, we have astigmatism (unequal phase centers in orthogonal planes). A horn has higher sidelobes in the $E$-plane than in the $H$-plane. Finally, the diffraction off $E$-plane walls causes backlobes. The aperture theory fails to predict them, but measurement or a GTD analysis shows them. Corrugating the walls can prevent all these problems.

Figure 7-7 shows the cross sections of two types of corrugated horns. The small-flare horn (*a*) is nominally the corrugated horn, and the wide-flare horn (*b*) is the scalar horn of Simmons and Kay [11]. Many papers on corrugated horns appear in Section VI of Love's [1] collection of papers. Thomas [12] provides a good design summary in a topic with many papers. The corrugations that extend circumferentially should be cut normal to the slant radius as in (*b*), but they may be cut normal to the axis (*a*) for small flare angles. Horns can be built either way, but when cut normal to the axis, the depth is different on the two sides.

The corrugated wall presents the same boundary conditions to the electric and magnetic fields when it is capacitive (slots $\lambda/4$ to $\lambda/2$ deep). When excited in the transition between the smooth-wall waveguide and the corrugated-wall cone, the $TE_{11}$ and $TM_{11}$ waveguide modes, have equal phase velocities. The combination of these

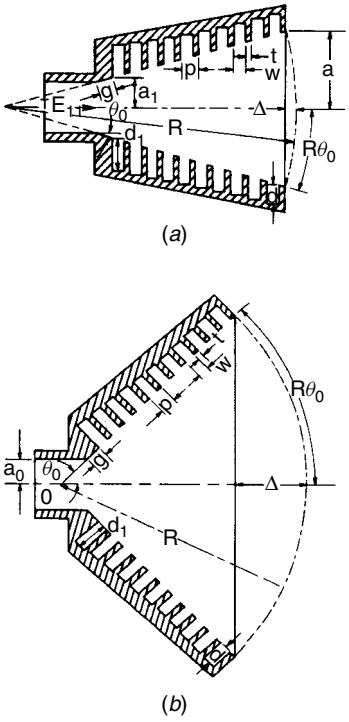


**FIGURE 7-7** (*a*) Corrugated horn; (*b*) scalar horn. (From [12], © 1978 IEEE.)

modes forms the hybrid mode $HE_{11}$ when the mode phases are equal. When the modes are out of phase by 180°, the hybrid mode is denoted $EH_{11}$. The ratio of the modes is called $\gamma$, and $\gamma = 1$ for the balanced $HE_{11}$ mode. $\gamma = 0$ corresponds to having only the $TM_{11}$ mode and $\gamma = \infty$ to having only the $TE_{11}$ mode. $\gamma = 1$ occurs when the corrugation depth is $\lambda/4$, but the horn parameters vary slowly with changing $\gamma$ [13]. We consider only $\gamma = 1$. Changing $\gamma$ has its biggest effect on the cross-polarization [12,14].

When $\gamma = 1$, the amplitude of the aperture fields is given by [15]

$$E_\rho = J_0\left(\frac{x_{01}\rho}{a}\right)\cos\phi_c$$
$$E_\phi = -J_0\left(\frac{x_{01}\rho}{a}\right)\sin\phi_c \tag{7-21}$$

where $x_{01} = 2.405$ is the first zero of $J_0(x)$, the Bessel function. The fields vanish at the walls and prevent edge diffractions that produce sidelobes and backscatter. The lower-order slope diffractions still produce small sidelobes and backlobes, but we get $H$-plane-type lobes in all planes. In amplitude the aperture fields are symmetrical about the axis and all patterns through the cone axis are identical.

A Huygens source analysis of the aperture fields with a quadratic phase distribution produces Figure 7-8, valid when the 10-dB beamwidth is less than 74° [12]. For greater beamwidths the flange changes the beamwidths of the small-aperture horn in the two planes and we should use the scalar horn. Table 7-6 lists the 3-, 10-, and 20-dB points

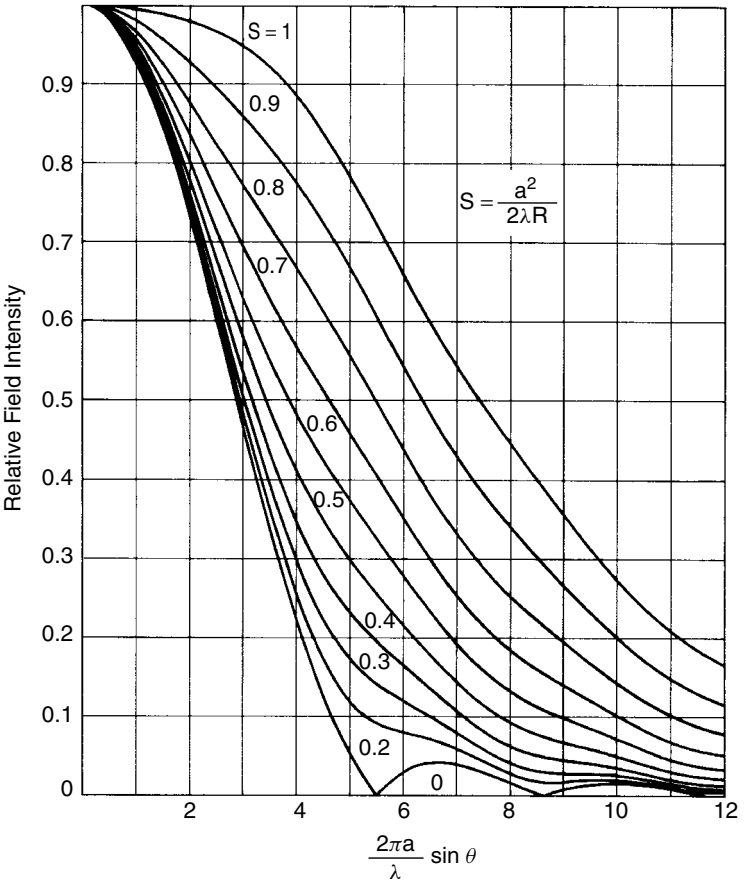


**FIGURE 7-8** Universal pattern of a circular corrugated horn: $HE_{11}$ mode.

**TABLE 7-6 Resonant Circular Corrugated Horn Beamwidth Points $(2\pi a/\lambda)\sin\theta$, $HE_{11}$ Mode**

| $S$ | 3 dB | 10 dB | 20 dB | ATL + PEL (dB) | $S$ | 3 dB | 10 dB | 20 dB | ATL + PEL (dB) |
|---|---|---|---|---|---|---|---|---|---|
| 0.00 | 2.0779 | 3.5978 | 4.6711 | 1.60 | 0.52 | 2.3688 | 4.9532 | 7.9936 | 4.04 |
| 0.04 | 2.0791 | 3.6020 | 4.6878 | 1.62 | 0.56 | 2.4411 | 5.2720 | 8.4261 | 4.44 |
| 0.08 | 2.0827 | 3.6150 | 4.7405 | 1.66 | 0.60 | 2.5317 | 5.5878 | 8.9472 | 4.86 |
| 0.12 | 2.0887 | 3.6371 | 4.8387 | 1.73 | 0.64 | 2.6469 | 5.8913 | 9.4352 | 5.31 |
| 0.16 | 2.0974 | 3.6692 | 5.0061 | 1.83 | 0.68 | 2.7966 | 6.1877 | 9.8514 | 5.79 |
| 0.20 | 2.1088 | 3.7129 | 5.3052 | 1.96 | 0.72 | 2.9946 | 6.4896 | 10.2337 | 6.30 |
| 0.24 | 2.1234 | 3.7699 | 5.8451 | 2.12 | 0.76 | 3.2597 | 6.8134 | 10.6250 | 6.83 |
| 0.28 | 2.1415 | 3.8433 | 6.3379 | 2.30 | 0.80 | 3.6061 | 7.1788 | 11.0735 | 7.39 |
| 0.32 | 2.1637 | 3.9372 | 6.6613 | 2.52 | 0.84 | 4.0189 | 7.6042 | 11.6356 | 7.96 |
| 0.36 | 2.1906 | 4.0572 | 6.9179 | 2.76 | 0.88 | 4.4475 | 8.0852 | 12.2658 | 8.54 |
| 0.40 | 2.2231 | 4.2112 | 7.1534 | 3.04 | 0.92 | 4.8536 | 8.5773 | 12.8236 | 9.13 |
| 0.44 | 2.2624 | 4.4090 | 7.3939 | 3.34 | 0.96 | 5.2331 | 9.0395 | 13.3059 | 9.72 |
| 0.48 | 2.3103 | 4.6578 | 7.6633 | 3.68 | 1.00 | 5.5984 | 9.4701 | 13.7706 | 10.29 |

from Figure 7-8. We use the table to find beamwidths of given horns or design to given beamwidths. Table 7-6 also lists the sum of ATL and PEL(GF) for various $S$. We estimate gain or design to a given gain with this listing.

***Example*** Calculate 10-dB beamwidth and gain of a corrugated conical horn with an aperture radius of 12 cm and a slant radius of 50 cm at 5 GHz:

$$S = \frac{a^2}{2\lambda R} = \frac{12^2}{2(6)(50)} = 0.24$$

From Table 7-7 we read the $k$-space value at 10 dB for $S = 0.24$:

$$\frac{2\pi a}{\lambda} \sin\theta = 3.7699 \quad \text{or} \quad \theta = 17.46^\circ$$

We include the obliquity factor, since the pattern loss will be greater than 10 dB at $\theta = 17.46^\circ$:

$$(1 + \cos 17.46^\circ)/2 : -0.20\,\text{dB} \qquad \text{BW}_{10} = \sqrt{\frac{10}{10.20}}34.92^\circ = 34.57^\circ$$

A smooth-wall horn with the same dimensions has a similar $H$-plane beamwidth (33.4°).

We calculate gain from the distribution losses and aperture area:

$$\text{GF} = \text{ATL} + \text{PEL} = 2.12\,\text{dB} \qquad \text{gain} = 20\log\frac{\pi D}{\lambda} - \text{GF} = 19.86\,\text{dB}$$

The smooth-wall horn has about 0.5 dB more gain (20.4 dB).

***Example*** Design a circular corrugated-wall horn at 8 GHz with a gain of 22 dB.

We use Eq. (7-20) with the GF from Table 7-6. Choose $S = 0.20$ (arbitrary):

$$D = \frac{3.75\,\text{cm}}{\pi} \cdot 10^{(22+1.96)/20} = 18.83\,\text{cm}$$

$$R = \frac{D^2}{8\lambda S} = 59.10\,\text{cm}$$

**TABLE 7-7 Phase-Center Axial Location of a Circular Corrugated Horn ($HE_{11}$ Mode) Behind the Aperture as a Ratio of the Slant Length**

| $S$ | $L_p/R$ | $S$ | $L_p/R$ |
|---|---|---|---|
| 0.00 | 0.0 | 0.36 | 0.386 |
| 0.04 | 0.005 | 0.40 | 0.464 |
| 0.08 | 0.020 | 0.44 | 0.542 |
| 0.12 | 0.045 | 0.48 | 0.614 |
| 0.16 | 0.080 | 0.52 | 0.673 |
| 0.20 | 0.124 | 0.56 | 0.718 |
| 0.24 | 0.178 | 0.60 | 0.753 |
| 0.28 | 0.240 | 0.64 | 0.783 |
| 0.32 | 0.310 | 0.68 | 0.811 |

The phase center, like that of other horns, starts at the aperture for $S = 0$ ($R = \infty$) and moves toward the apex as $S$ increases. Table 7-7 lists the phase-center location as a ratio of the slant radius. Because the aperture distribution is the same along all radial lines of the aperture, the phase center is the same in all planes. We measure some variation, since the balance between modes will not be perfect, and some higher-order modes will be generated. The phase center moves least over a frequency band for long horns (small $S$). A wide-flare-angle horn has its phase center at the apex and is better described as a scalar horn.

### 7-3.1 Scalar Horn

A scalar horn has a wide half-flare angle, $\theta_0$. Its beamwidth depends on the half-flare angle. Since the phase distribution in the aperture is large, there is an optimum diameter for a given flare angle. Table 7-8 lists the optimum diameter versus the flare angle. The beamwidth is approximately a linear function of the half-flare angle, $\theta_0$, for the optimum horn:

$$\begin{aligned} \mathrm{BW}_{3\,\mathrm{dB}} &= 0.74\theta_0 \\ \mathrm{BW}_{10\,\mathrm{dB}} &= 1.51\theta_0 \\ \mathrm{BW}_{20\,\mathrm{dB}} &= 2.32\theta_0 \end{aligned} \tag{7-22}$$

A scalar horn has a wider bandwidth as a reflector feed than that of a small-flare-angle corrugated horn, because the phase center is fixed at the horn apex.

### 7-3.2 Corrugation Design

The corrugations present a capacitive reactance to the passing wave. When a corrugated surface is inductive, it will support surface waves. The depth of corrugations must be between $\lambda/4$ and $\lambda/2$. Less than $\lambda/4$ or greater than $\lambda/2$, it is inductive. Between $3\lambda/2$ and $\lambda$ it will be capacitive again, but this second passband is seldom used. A quarter-wavelength corrugation depth balances the two modes and gives the best results. The corrugations need be only $\lambda/4$ at the aperture. Before the aperture we find it better to deepen the slots. Quarter-wavelength-deep corrugations mismatch the horn in the transition region, where the $TM_{11}$ mode is generated from the $TE_{11}$ mode and depths approaching $\lambda/2$ have the least effect on match.

**TABLE 7-8 Optimum Diameter of a Scalar Horn**

| Half-Flare Angle, $\theta_0$ (deg) | Aperture Diameter ($\lambda$) | Half-Flare Angle, $\theta_0$ (deg) | Aperture Diameter ($\lambda$) |
|---|---|---|---|
| 15 | 10.5 | 45 | 3.5 |
| 20 | 8.0 | 50 | 3.0 |
| 25 | 6.4 | 55 | 2.8 |
| 30 | 5.2 | 60 | 2.6 |
| 35 | 4.5 | 65 | 2.4 |
| 40 | 3.9 | 70 | 2.3 |

*Source*: [16, p. 429].

To design for a particular band, limited to about 1.5 : 1 for a good match, we design with tapered corrugation depths. We make the corrugations $\lambda/4$ deep at the aperture at the low-frequency end. The high-frequency band edge determines the corrugation depth at just short of $\lambda/2$ in the throat. The horn needs at least four corrugations per wavelength along the slant radius. The high-frequency end determines the corrugation spacing. The first few corrugations can be used to match the horn to the waveguide, and we can improve the match by shaping the corrugation widths [14]. The slots should be as wide as practical spacers will allow. Mechanical considerations, such as shock and vibration, will determine the limits on the thinness of spacers, but corrugations greatly increase the strength of the bell.

The circular geometry of the horn changes the corrugation depth necessary for the balanced $HE_{11}$ mode from $\lambda/4$. An empirical formula for the depth is given by [17]

$$d = \frac{\lambda}{4} \exp\left(\frac{1}{2.5\ ka}\right) \qquad ka > 2 \tag{7-23}$$

We increase the depth slightly at the horn aperture.

### 7-3.3 Choke Horns

We can place corrugations in the flanges of small-aperture horns and design wide-beamwidth antennas with good pattern symmetry and low cross-polarization. The choke horn (Figure 7-9) is the limit of a scalar horn opened to $\theta_0 = 90°$. The corrugations consist of concentric rings about the aperture and are generally a quarter-wavelength deep. The best location for the corrugated rings may not be in the same plane as the aperture but instead somewhat behind as reported for a feed for $f/D = 0.3$ reflector [18;19, pp. 200–209].

The design for the reflector feed [18] used four corrugations. James [20] and Kumer [21] show that using only one corrugation is quite effective. More corrugations improve the design but only add marginally. Small apertures need the corrugations to reduce the cross-polarization that peaks in the diagonal planes between the $E$- and $H$-planes.

We usually assume a Huygens source in the aperture plane of the horn. This approximation collapses as we shrink the aperture to achieve wide beamwidths. In the limit

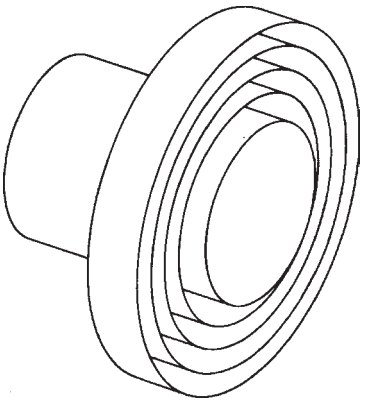

**FIGURE 7-9** Choke horn.

we have only a slot analyzed from magnetic currents replacing the electric field in the aperture. The magnetic field is ignored in the slot while a Huygens source assumption is that the ratio of the electric to magnetic field is the same as the impedance of free space. Waveguides have high wave impedances, which implies small magnetic fields. To calculate the far field, Eq. (2-23) must be used with the actual ratio of fields in the aperture instead of Eq. (2-24), with its Huygens source approximation. Restricting the aperture dimensions to achieve wide beamwidths will limit the bandwidth as well as the cross-polarization isolation, because reducing volume raises $Q$.

### 7-3.4 Rectangular Corrugated Horns

We can design rectangular horns with corrugated walls, but we only need to cut corrugations in the $E$-plane walls to produce a cosine distribution in the $E$-plane. Only for dual polarization do we need corrugations in the $H$-plane walls. We analyze the horn as having an $H$-plane distribution (cosine) in both planes and use the results of Section 7-1. The larger aperture dimension in the diagonal plane decreases the beamwidth slightly, but the rectangular horn still provides an acceptable design. Both planes have a linear amplitude taper loss of 0.91 dB. We use the cosine column of Table 4-42 for the quadratic phase error loss. We design beamwidths using Table 7-1. Equalizing the distributions in both planes of square horns results in equal phase centers, given by Table 7-3 ($H$-plane).

***Example*** Compute the gain of a square corrugated horn with an aperture width of 24 cm and a slant radius of 50 cm at 5 GHz.

From Eq. (7-1),

$$S = \frac{W^2}{8\lambda R} = \frac{24^2}{8(6)(50)} = 0.24$$

We use the cosine column of Table 4-42 for the phase error loss: $\text{PEL}_x = \text{PEL}_y = 0.42$ (cosine). The amplitude taper loss is the same in both planes: 0.91 dB.

$$\begin{aligned}\text{Gain} &= 10\log\frac{4\pi W^2}{\lambda^2} - \text{ATL}_x - \text{ATL}_y - \text{PEL}_x - \text{PEL}_y \\ &= 23.03 - 0.91 - 0.91 - 0.42 - 0.42 = 20.4\,\text{dB}\end{aligned}$$

A circular corrugated horn with a diameter equal to the width and having the same slant radius has a gain of 19.9 dB or 0.5 dB less. The larger aperture area increases the gain over the circular horn.

## 7-4 CORRUGATED GROUND PLANE

The corrugated surface (Figure 7-10) supports surface waves (TM) when the slot depth is less than $\lambda/4$ (inductive). As with the corrugated horn, we assume many slots per wavelength along the direction of propagation. The fields attenuate exponentially above the ends of the corrugations in a surface wave. We derive the fields from a potential function

$$\psi = A_1 \exp\left(\frac{-2\pi bx}{\lambda}\right)\exp(-jk_z z) \tag{7-24}$$

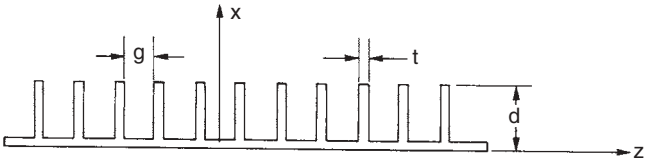


**FIGURE 7-10** Corrugated ground plane.

above the corrugations, where $A_1$ is an amplitude constant, $x$ the distance out of the corrugations, and $\alpha(= 2\pi b/\lambda)$ the attenuation constant of the fields above the corrugations. We expand the fields and take the ratio of the $z$-directed electric field to the $y$-directed magnetic field to find the wave impedance into the corrugated surface:

$$E_z = \frac{1}{j\omega\varepsilon_0}(k^2 - k_z^2)\psi = -\left(\frac{2\pi b}{\lambda}\right)^2 \frac{A_1}{j\omega\varepsilon_0} \exp\left(-\frac{2\pi b}{\lambda}\right) \exp(-jk_z z)$$

$$H_y = -\frac{\partial\psi}{\partial x} = \frac{2\pi b}{\lambda} A_1 \exp\left(-\frac{2\pi b}{\lambda}\right) \exp(-jk_z z)$$

$$Z_{-x} = \frac{E_z}{H_y} = \frac{j(2\pi b/\lambda)}{\omega\varepsilon_0} = \frac{j(2\pi b/\lambda)\sqrt{\mu_0}}{\omega\sqrt{\varepsilon_0\mu_0}\sqrt{\varepsilon_0}} = \frac{j(kb)}{k}\eta = jb\eta \tag{7-25}$$

where $\eta$ is the impedance of free space and $b$ is related to $\alpha$ [Eq. (7-24)]. The structure must present this impedance to the wave. The corrugated surface is a parallel-plate transmission line to $E_z$, and it presents a per unit length impedance of

$$Z_c = j\eta \tan kd \tag{7-26}$$

where $d$ is the corrugation depth. We equate Eqs. (7-25) and (7-26) to determine the constant $b$:

$$b = \tan kd \tag{7-27}$$

We use Eq. (7-27) in Eq. (10-16) for the relative propagation constant:

$$P = \sqrt{1 + b^2} = \sqrt{1 + \tan^2 kd} \tag{7-28}$$

We include the effect of the corrugation thickness by averaging between the parallel-plate impedance and the zero impedance along the corrugation edges. Equation (7-28) becomes

$$P = \sqrt{1 + \left(\frac{g}{g+t}\right)^2 \tan^2 kd} \tag{7-29}$$

where $g$ is the gap distance and $t$ is the corrugation thickness. $P$ increases without bound as the depth $d$ approaches $\lambda/4$. The fields become tightly bound to the surface and attenuate rapidly to zero above the corrugations—the normal electric field vanishes as in a corrugated horn $E$-plane wall. We design the depth of the corrugations by using

$$d = \frac{\lambda}{2\pi} \tan^{-1} \frac{g+t}{g\sqrt{P^2 - 1}} \tag{7-30}$$

When the corrugation depth approaches $\lambda/4$, the surface impedance [Eq. (7-26)] approaches infinity and the tangential magnetic field vanishes on the surface to create an artificial PMC (Section 2-3) for waves polarized along the $z$-axis. The reflection coefficient is $+1$ instead of $-1$ for the PEC surface. Waves polarized along the $y$-axis encounter closely spaced corrugations that approximately produce a PEC surface with the usual metal wall reflection coefficient of $-1$. Whereas a PEC reflects an incident circularly polarized wave with opposite sense of circular polarization, the artificial PMC (soft) surface [22, pp. 276–280] reflects the wave with the same sense of polarization. We can use these surfaces to shape the pattern of a wide-beamwidth circularly polarized antenna to narrow the beamwidth without generating the opposite sense polarization, which would be generated by metal walls.

A ground plane covered with circular coaxial corrugations $\lambda/4$ deep reduces the edge diffraction that produces a large backlobe for a monopole antenna mounted in the center (Figure 5-23). The artificial soft wall causes the reduction of circumferential magnetic fields and the associated GTD diffraction (Section 2-7.11) [23]. This increases the forward gain by reducing the backlobe. It is not necessary to corrugate the entire top surface. Figure 7-11 illustrates a surface with only two coaxial corrugations around the outer rim. These reduce the backlobe for a dipole mounted over the ground plane without generating significant cross-polarization from a pair of orthogonal dipoles fed for a circular polarization. Corrugating the entire surface would cause radiation of cross-polarization because the region below the dipole pair radiates oppositely sensed circular polarization. The corrugated surface reflects the same sense of circular polarization as incident. The PEC surface reverses the sense of circular polarization of the reflected wave and both waves add. The corrugations only reduce the backlobe. The choke horn uses the same type of corrugations to reduce the backlobe radiated from the small-diameter horn aperture.

The corrugations can be placed radially below the ground plane by using short-circuited radial transmission lines (Figure 7-12) and also reduce the backlobe. We

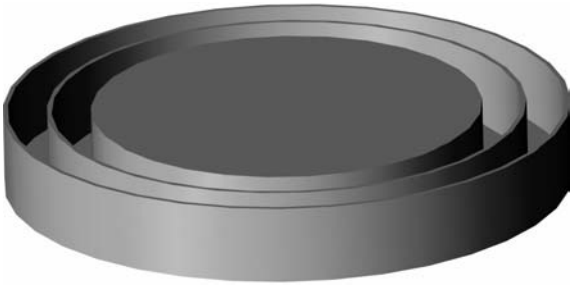

**FIGURE 7-11** Ground plane with two coaxial corrugations to reduce edge diffraction.

**FIGURE 7-12** Ground plane with short-circuited radial transmission-line corrugations.

**TABLE 7-9 Radial Transmission Outer Choke Depth at Resonance**

| Outer Radius (λ) | Depth (λ) | Outer Radius (λ) | Depth (λ) |
|---|---|---|---|
| 0.25 | 0.188 | 0.70 | 0.230 |
| 0.30 | 0.199 | 0.80 | 0.233 |
| 0.35 | 0.208 | 1.0 | 0.236 |
| 0.40 | 0.213 | 2.0 | 0.243 |
| 0.50 | 0.222 | 4.0 | 0.247 |
| 0.60 | 0.227 | | |

compute the reactance at the outer radius from the following equation, which uses Bessel and Neumann functions:

$$X = j\frac{\eta b}{2\pi r}\frac{N_0(kr)J_0(kr_o) - J_0(kr)N_0(kr_o)}{J_1(kr)N_0(kr_o) - N_1(kr)J_0(kr_o)}$$

The short-circuited wall is located at radius $r_o$ and the spacing between the plates is $b$. Reactance $X$ grows rapidly as $r$ approaches resonance. For a large outer radius the difference $r - r_o$ approaches λ/4 but is less for a small radius. Table 7-9 gives the difference in radius versus the outer radius for resonance.

Corrugations on the upper surface are more effective than radial corrugations, but the radial line chokes fit easily behind a small ground plane. In both cases the corrugations enhance radiation behind the ground plane at frequencies below resonance λ/4 depths, because a surface wave is generated along the corrugations. Corrugated surfaces are useful structures because they can be used to enhance or reduce radiation, depending on their depth.

## 7-5 GAUSSIAN BEAM

Corrugated horns and simple reflector feeds can be approximated with Gaussian beams. An infinite circularly symmetrical Gaussian aperture distribution located in the $x-y$ plane radiates a Gaussian beam along the $z$-axis. The radial exponent of the Gaussian distribution determines the spread of the wave as it propagates along the $z$-axis. We use the distribution to calculate the radiation pattern and then add the Huygens source (Section 2-2.2) for polarization. The analysis is divided into far- and near-field approximations. The near-field approximation consists of a paraxial wave. The Gaussian beam satisfies Maxwell's equations by using the free-space Helmholtz equation and produces correct patterns when applied with physical optics (PO).

The free-space Green's function satisfies the Helmholtz equation: $e^{-jkR}/R$. We derive the Gaussian beam from a point source placed at a complex position along the $z$-axis: $z_0 = -jb$. A source at this position produces a Gaussian distribution in the $z = 0$ plane.

$$\exp\left(\frac{-\rho^2}{W_0^2}\right) \quad \text{with} \quad \rho^2 = x^2 + y^2$$

$W_0$ is the beam waist radius where amplitude has dropped by $1/e$. We relate the waist radius $W_0$ to the position $b$ by [24, pp. 80–90]

$$W_0^2 = \frac{2b}{k} \qquad \text{where} \quad k = \frac{2\pi}{\lambda}$$

As the wave propagates along the $z$-axis, its amplitude retains the Gaussian distribution in the radial direction $\rho$ but the waist spreads:

$$W^2(z) = W_0^2 \left[1 + \left(\frac{z}{b}\right)^2\right]$$

The waist surface is a hyperboloid with a ring focus at radius $b$ located at $z = 0$. The wave amplitude reduces by the ratio of the waists and combines with the radial Gaussian distribution:

$$\frac{W_0}{W(z)} \exp\left[-\frac{\rho^2}{W^2(z)}\right]$$

The phase of the paraxial (near-field) wave has two terms. The first is the normal $z$-directed wave phase $\exp(-jkz)$ and the second is a quadratic phase term that arises from the complex location of the point source at $z = -jb$. The quadratic phase term slant radius depends on the location along the $z$-axis:

$$R_c(z) = z\left[1 + \left(\frac{b}{z}\right)^2\right]$$

The paraxial Gaussian beam has an additional slippage phase term $\zeta(z) = \tan^{-1}(z/b)$. The paraxial Gaussian beam phase term is the sum

$$\exp\left[-jkz - jk\frac{\rho^2}{2R_c(z)} + j\zeta(z)\right]$$

The constant phase (eikonal) surfaces between the hyperboloid amplitude surfaces are ellipsoids with a ring focus at radius $b$ located at $z = 0$. At $z = 0$ the eikonal surface is planar. We combine the amplitude and phase terms for the complete paraxial Gaussian beam equation:

$$-jE_0 \cos^2\frac{\theta}{2}\frac{W_0}{W(z)} \exp\left[-\frac{\rho^2}{W^2(z)}\right] \exp\left[-jkz - jk\frac{\rho^2}{2R_c(z)} + j\zeta(z)\right] \times (\hat{\theta}\cos\phi - \hat{\phi}\sin\phi) \tag{7-31}$$

The Huygens source polarization for an $x$-directed wave [Eq. (1-38)] and the obliquity factor [Eq. (2-14)] have been added to Eq. (7-31). We determine the constant $E_0$ by equating the radiation between this paraxial beam and the far-field expression for a Gaussian beam with a given input power. The recommended distance to equate the two representations is $z = 200W_0^2/\lambda$.

We calculate the far-field Gaussian beam by substituting the point source position into $e^{-jkR}/R$ and approximating $R$ with a far-field expression [25, pp. 96–106]:

$$R = \sqrt{x^2 + y^2 + z^2 - b^2 + j2bz} = \sqrt{r^2 - b^2 + j2br\cos\theta} \tag{7-32}$$

In the far field we can ignore $b^2$ and expand Eq. (7-32) in a Taylor series and retain the first two terms, which reduces $e^{-jkR}/R$ to $e^{kb\cos\theta}e^{-jkr}/r$. We combine this term with the Huygens source radiation to produce the far-field Gaussian beam equation for an $x$-directed linear polarization in the aperture normalized at $\theta = 0$ to directivity:

$$\mathbf{E}(r,\theta,\phi) = \sqrt{\frac{P_0 \cdot \text{directivity} \cdot \eta}{4\pi}} \cos^2\frac{\theta}{2} e^{kb(\cos\theta - 1)}(\hat{\theta}\cos\phi - \hat{\phi}\sin\phi)\frac{e^{-jkr}}{r} \tag{7-33}$$

The directivity is found by integrating the pattern of Eq. (7-33):

$$\text{directivity} = \frac{4(2\,kb)^2}{2(2\,kb) - 2 + 1/(2\,kb) - e^{-2(2\,kb)}/(2\,kb)} \tag{7-34}$$

Scale 7-7 gives the relationship between gain and the 10-dB beamwidth for a Gaussian beam.

Given the beamwidth (BW) at a given level $L$(dB), we solve Eq. (7-33) for the complex-plane point source position $b$:

$$b = \frac{2\log[\cos(\text{BW}/4)] + |L/20|}{k[1 - \cos(\text{BW}/2)]\log e} \tag{7-35}$$

Scale 7-8 relates Gaussian beam half-depth of focus, $b$, to its 10-dB beamwidth, and Scale 7-9 gives the minimum waist diameter.

We simplify the expression for the Gaussian beam for small angles by expanding $\cos\theta$ in a Taylor series $\cos\theta \approx 1 - \theta^2/2$, which reduces Eq. (7-33):

$$\mathbf{E}(r,\theta,\phi) = E_0\cos^2\frac{\theta}{2} e^{-(\theta/\theta_0)^2}(\hat{\theta}\cos\phi - \hat{\phi}\sin\phi)\frac{e^{-jkr}}{r} \tag{7-36}$$

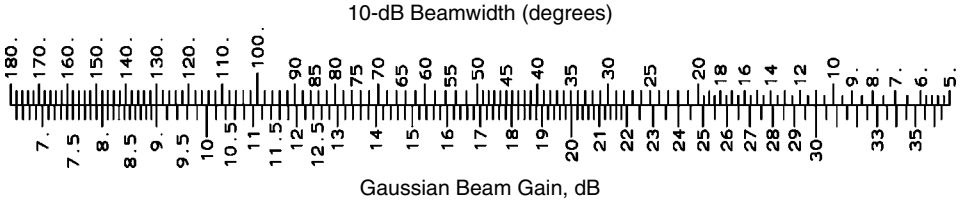


**SCALE 7-7** Gaussian beam gain compared to a 10-dB beamwidth.

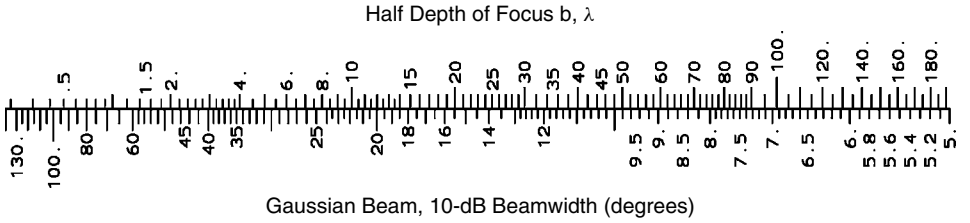


**SCALE 7-8** Gaussian beam half-depth of focus, $b$, compared to a 10-dB beamwidth.

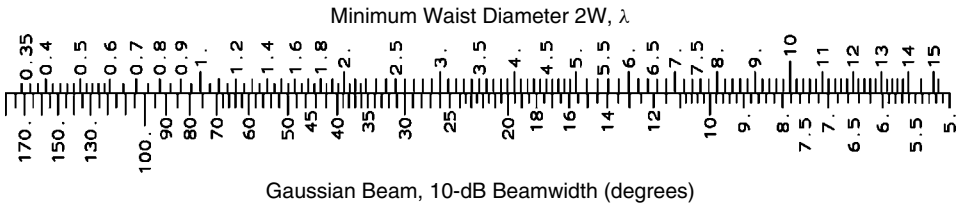


**SCALE 7-9** Gaussian beam minimum waist diameter compared to a 10-dB beamwidth.

The angle $\theta_0$ is the beam divergence [24, pp. 80–90], given by

$$\theta_0 = \frac{2}{kW_0} = \sqrt{\frac{2}{kb}}$$

Equation (7-36) cannot be used beyond $\theta_0$ because it is based on a small-angle approximation.

We can use a Gaussian beam to approximate the pattern of a corrugated horn [26, pp. 170–176]. The minimum waist is located behind the horn aperture $L_p$, the phase-center distance given the aperture radius $a$ and the slant radius $R$:

$$L_p = \frac{R}{1 + [2R/k(0.644a)^2]^2} \tag{7-37}$$

$L_p$ is the location of $z = 0$ of the Gaussian beam. The minimum waist radius $W_0$ is given by

$$W_0 = \frac{0.644a}{1 + [k(0.644a)^2/2R]^2} \qquad b = \frac{W_0^2 k}{2} \tag{7-38}$$

For a 22 dB-gain corrugated horn, Eq. (7-38) produces a Gaussian beam with the same gain as the horn for $S = 0.134$. For different values of $S$, Eq. (7-38) gives only approximate Gaussian beams to match the gain of corrugated horns. The Gaussian beam has a 10-dB beamwidth of 27.5° and the corrugated horn has a beamwidth of 27.2°. The phase center of the Gaussian beam given by Eq. (7-37) is 2.44λ behind the aperture and the actual horn phase center is at 0.89λ. The Gaussian beam approximation finds the near-field pattern of the corrugated horn because it includes the finite waist size instead of assuming a point source at the phase center of the horn. A PO analysis using the equivalent currents in the aperture [27, pp. 141–156] also finds the near-field pattern but requires greater calculation effort.

## 7-6 RIDGED WAVEGUIDE HORNS

Inserting ridges in the $E$-plane of a waveguide lowers the cutoff frequency compared to a waveguide of the same width. The ridges raise the cutoff frequencies of the next two higher modes and can produce a waveguide that operates over a 10 : 1 frequency range or more. If we use this as the input waveguide to a horn and taper the ridges until they do not block the horn aperture, the horn radiates a pattern similar to the smooth-wall horn. Near the aperture the horn can support many higher-order waveguide modes

as frequency increases. The horn generates some higher-mode content to the fields which distorts the pattern over narrow frequency ranges, but for many applications such distortions are acceptable. Initial designs [28] used dual ridges for a single linear polarization, while later designs increased the number of ridges to four (quad-ridge) to allow for dual linear (or circular) polarization.

Design concentrates on the input waveguide dimensions. We apply transverse resonance to the waveguide to calculate its cutoff frequencies. A rectangular waveguide with the electric field parallel to the narrow wall can be considered as a parallel-plate transmission line with the wave traveling between the two narrow wall shorts at cutoff (see Section 5-24). The parallel-plate transmission-line impedance is $\eta b$ for a height of $b$ (meters). The lowest-order mode cutoff frequency for a normal rectangular waveguide occurs when the width $a = \lambda/2$. The transverse resonance method considers half the width as a transmission line and cutoff occurs when the impedance at the centerline is an open circuit (odd-order mode) or a short circuit (even-order mode) (i.e., $a/2 = N\lambda/4$) for mode $\mathrm{TE}_{N0}$. Of course, we ignore the impedance of the parallel-plate line because it is uniform.

Figure 7-13*a* shows the cross section of a dual-ridged waveguide. The diagram illustrates feeding the waveguide with a coaxial line running through the center of one ridge. The center conductor extends across the gap to feed the second ridge. The center pin does not need to touch the second ridge but can be coupled capacitively. The transverse resonance circuit of a dual-ridged horn used to determine cutoff frequencies consists of two transmission-line segments with a shunt capacitor due to the step. The capacitance depends on the ratio of the heights $\alpha = b_2/b_1$, where $b_2 < b_1$ [29]:

$$C = \frac{\varepsilon_0}{\pi}\left(\frac{\alpha^2+1}{\alpha}\cosh^{-1}\frac{1+\alpha^2}{1-\alpha^2} - 2\ln\frac{4\alpha}{1-\alpha^2}\right) \tag{7-39}$$

For the dual-ridged waveguide we analytically place a ground plane halfway across the waveguide $E$-plane and divide the waveguide into two half-height waveguides. Later we will consider the impedance, and the total impedance of the guide is these two

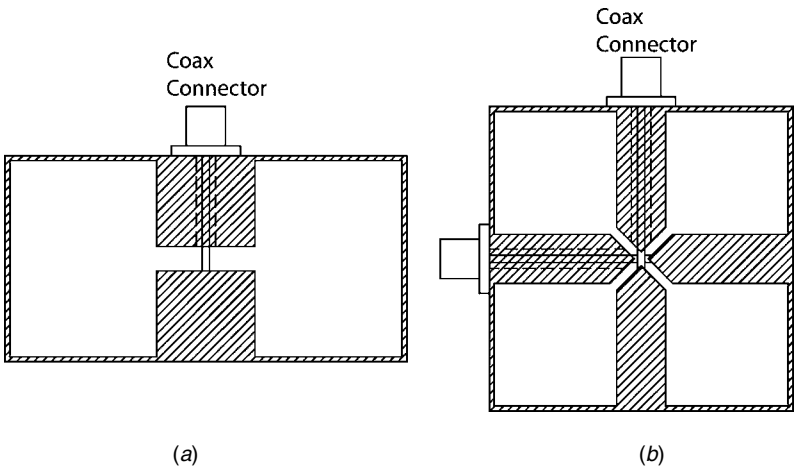


**FIGURE 7-13** Coaxial feeds of ridged waveguides: (*a*) dual ridge; (*b*) quad ridge.

half-height guides in series. Given the waveguide width $a_1$ and height $2b_1$, and the ridge width $a_2$ with gap $2b_2$, we solve for the cutoff frequency using a transcendental equation in admittance at the transition point between the two half-height waveguides. Odd-order TE modes have a virtual open circuit in the center of the ridge and a short circuit at the wall. Cutoff occurs for $k_c = 2\pi/\lambda_c = 2\pi f_c/c$ for $c$ equal to the speed of light [30]:

$$\frac{\tan(k_c a_2/2)}{\eta b_2} + k_c c C - \frac{\cot[k_c(a_1 - a_2)/2]}{\eta b_1} = 0 \tag{7-40}$$

We solve Eq. (7-40) numerically for $k_c$ for odd-order modes. The even modes have a virtual short circuit in the center, which leads to a similar equation for the cutoff number $k_c$:

$$-\frac{\cot(k_c a_2/2)}{\eta b_2} + k_c c C - \frac{\cot[k_c(a_1 - a_2)/2]}{\eta b_1} = 0 \tag{7-41}$$

We use Eq. (7-40) to calculate the cutoff wavelengths of modes $TE_{10}$ and $TE_{30}$ and Eq. (7-41) to compute the cutoff wavelength of mode $TE_{20}$ for given dimensions.

We design the waveguide to have a suitable low-frequency cutoff with an impedance equal to the input coax, whose outer conductor is connected to one ridge, with the center conductor jumping the gap to feed the other. The impedance at an infinite frequency is given by the equations

$$Y_\infty = \frac{1}{k\eta b_2}\left\{\frac{ka_2}{4} + \frac{\sin ka_2}{4} + \frac{b_2}{b_1}\frac{\cos^2(ka_2/2)}{\sin^2(ka_1/2)}\left(\frac{ka_1}{4} - \frac{\sin ka_1}{4}\right) + \frac{2b_2}{\lambda}\ln\left[\csc\left(\frac{\pi}{2}\frac{b_2}{b_1}\right)\cos^2\frac{ka_2}{2}\right]\right\}$$

$$Z_\infty = \frac{1}{Y_\infty} \tag{7-42}$$

The impedance at a finite frequency increases:

$$Z_0 = \frac{Z_\infty}{\sqrt{1 - (f_c/f)^2}} \tag{7-43}$$

An approximate value for the gap can be found from the impedance of microstrip. The infinite impedance equals slightly less than twice the impedance of microstrip the same width as the ridge with one-half the gap. The extra fringing capacitance between the sides of the ridges lowers the impedance compared to microstrip. You can use a microstrip line design program to find an approximate gap and a few evaluations of Eq. (7-42) to determine the correct gap. Design for $Z_\infty$ because the impedance approaches $Z_\infty$ rapidly as frequency increases by Eq. (7-43) and ridged horns operate over a large bandwidth.

Quad-ridged waveguide, illustrated in Figure 7-13*b*, requires modifications at the input to a horn. To achieve $Z_\infty = 50\,\Omega$, the gap must be reduced and the ridges made with a rooftop shape so that they fit within each other. The capacitance between the ridges for one polarization is a series combination of the two capacitors to the ridges for the second polarization. Similar to the dual-ridged waveguide, we divide the

waveguide along the centerline through the second set of ridges and analyze a single-ridged waveguide. Given a square waveguide with width $w$, ridge width $s$, and gap $g$ between the ridges of different polarizations, the equivalent single-ridged waveguide has parameters given by the expressions

$$a_1 = w + s(\sqrt{2} - 1) \qquad a_2 = s\sqrt{2}$$
$$b_1 = w - s/2 \qquad b_2 = g \tag{7-44}$$

For the quad-ridged waveguide the infinite impedance equals slightly less than four times the impedance of microstrip the same width as the equivalent ridge $a_2$ with one-half the gap. We use the parameters of Eq. (7-44) in Eqs. (7-39) through (7-43) to find the parameters of quad-ridged waveguide. Figure 7-13*b* demonstrates that the feed pin of one coax passes over the other to reduce coupling between them. The difference in distance to the waveguide shorting wall for the two coaxial lines produces different impedances for the two inputs.

We can use the expressions above for circular waveguides. We design with a width equal to the diameter. The infinite impedance is lower by the factor $\pi/4$. The cutoff frequency is about 1.25 times the cutoff frequency of the equivalent square waveguide [31].

Figure 7-14 gives a cross-sectional drawing of a ridged horn and demonstrates the key elements of design. A coax is fed through the center of one ridge and the center conductor jumps the gap and feeds the second ridge. We locate the coax close to the end of the ridge truncated before it reaches the waveguide back wall short circuit, leaving a small gap. Without ridges the waveguide is cutoff at the low-frequency end of the horn operation. Operating the waveguide below its cutoff frequency does not

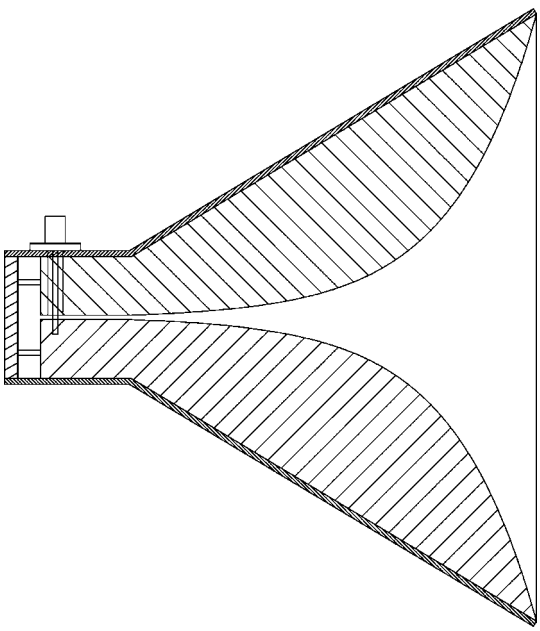

**FIGURE 7-14** Dual-ridged waveguide horn cross section.

prevent the wave from reaching the back wall because the distance is short. The original horns [28] used waveguides in cutoff at the feed point at the lowest frequencies. By tapering the sidewalls the waveguide operates above cutoff in a short distance from the feed and the waves propagated to that region. Cutoff only means that a wave will not propagate in a long waveguide, but it attenuates as it moves along the waveguide. Figure 7-14 shows optional shorting pins between the back wall and the ridges. These prevent an additional resonance in impedance that may arise at a frequency when the height of a single ridge approaches $\lambda/2$. Not all designs need these pins.

We space the ridges to form a transmission line matched to the feed coax at the input. A uniform section of ridged waveguide extends to the throat of the horn. The horn shown in Figure 7-14 uses an exponentially tapered ridge that has an additional linear taper with slope 0.02 [28] empirically found to improve the impedance match. It would seem that designing a classical tapered impedance transformer would give a better impedance match, but the simple exponential physical taper produces an excellent impedance match. The gain of the horn falls short of the equivalent open horn because multiple modes are excited and beamwidth broadens. In a dual-ridged horn the power concentrates between the ridges in the $E$-plane, and we can replace the $H$-plane sidewalls with a few rods. We space the rods close enough to block radiation at the lower frequencies and allow high-frequency radiation through the spaces. Since the fields are concentrated between the ridges at high frequencies, the side $H$-plane walls have little effect on the pattern. A quad-ridged horn requires solid walls.

A circular quad-ridged horn was measured as a possible feed for a Cassegrain reflector from 6 to 18 GHz. The horn has a 13.2-cm aperture diameter and a 37.6-cm slant radius and operates from 2 to 18 GHz. Figure 7-15 plots the measured $E$- and $H$-plane 10-dB beamwidths along with the beamwidths of both smooth and corrugated wall horns of the same size. Neither smooth wall nor corrugated wall horns could be designed to operate over this wide bandwidth; they are shown only for comparison. The

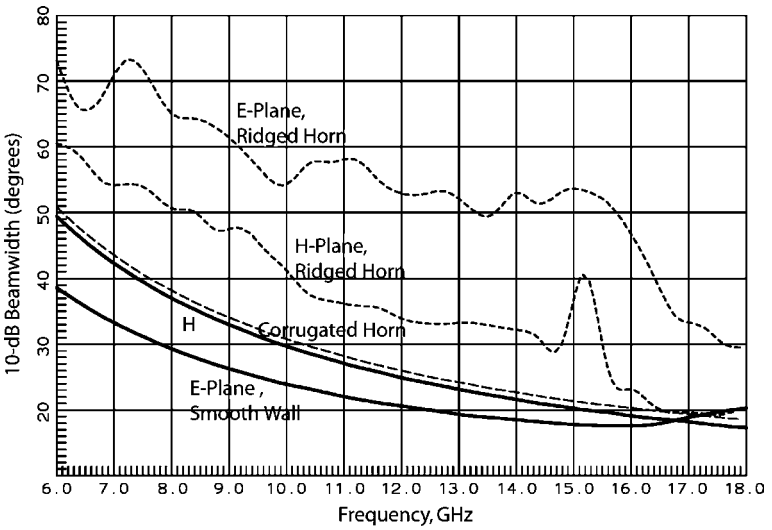


**FIGURE 7-15** Measured 10-dB beamwidths of a circular quad-ridged horn compared to the calculated beamwidths of smooth- and corrugated-wall horns.

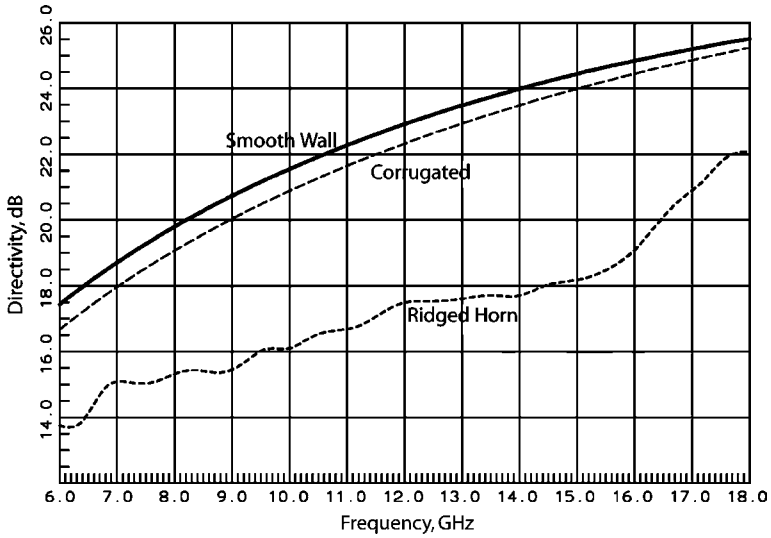


**FIGURE 7-16** Measured directivity of a circular quad-ridged horn compared to those of smooth- and corrugated-wall horns.

quad-ridged horn has wider beamwidths in both planes compared to the other horns. This reduces the gain shown in Figure 7-16. Similar to the corrugated horn, the quad-ridged horn operates with multiple modes. We can determine the circular waveguide modes radiated by using physical optics analysis on the measured pattern. We radiate a plane wave into a circular aperture plane equal to the physical horn aperture and placed at the average phase center. Each plane wave, weighted by the pattern level and sin $\theta$, excites Huygens source currents on the patches that cover the aperture by using Eq. (2-33). We normalize the currents to 1 watt and project the currents for each mode of a circular waveguide horn onto the incident wave currents by integrating over the aperture to determine their excitation levels $b_m$:

$$b_m = \iint_S \mathbf{J}_a \cdot \mathbf{J}_m^* \, dS \tag{7-45}$$

We use the aperture currents $\mathbf{J}_a$ and mode currents $\mathbf{J}_m$ in Eq. (7-45), where we take the complex conjugate of the vector for projection in the same manner as polarization calculations (section 1-11). We operate on the electric currents only because the magnetic currents are proportional to the electric currents for Huygens sources. Figure 7-17 plots the levels of the $TE_{11}$, $TM_{11}$, and diagonally oriented $TE_{21}$ modes. $TE_{11}$ and $TM_{11}$ modes are also excited in a corrugated horn, but the level of the $TM_{11}$ mode is approximately $-5$ dB relative to the $TE_{11}$ mode. Further measurements of the horn show that it has approximately equal power in the $TE_{11}$ and $TM_{11}$ modes, all the way down to 2.7 GHz. Below that frequency the horn aperture will not support the $TM_{11}$ mode and the pattern reverts to the $TE_{11}$ mode only, which narrows the beamwidth. Analysis shows that the diagonally oriented $TE_{21}$ mode peaks at an angle halfway around from the ridges and increases cross-polarization in the diagonal plane. The unmatched beamwidths in the $E$- and $H$-planes also increases the Huygens source

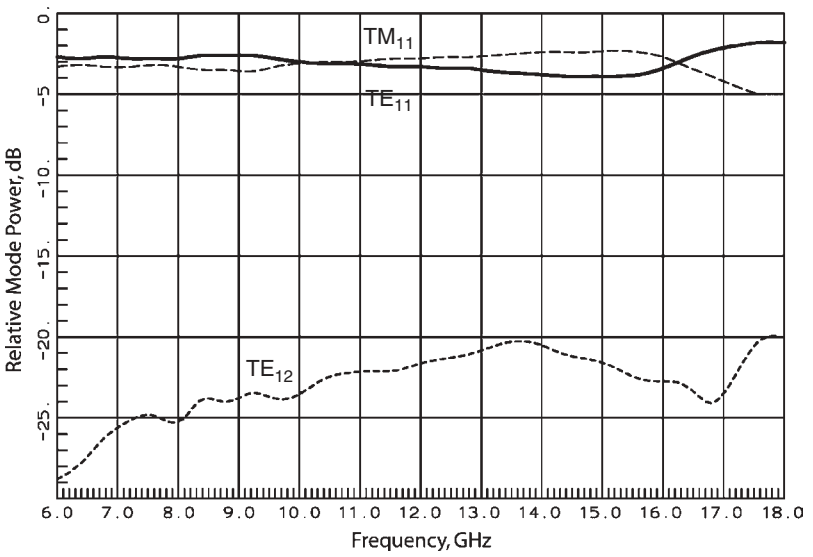


**FIGURE 7-17** Modal decomposition into circular waveguide modes of the measured pattern of a circular quad-ridged horn.

cross-polarization (section 1-11.2) in the diagonal plane. Square quad-ridged horns have similar modes. Measurements on a 63.5-cm-square aperture horn with a 140-cm slant length produced nearly equal levels of $TE_{10}$ and $TM_{12}$ modes, similar to the $TE_{11}$ and $TM_{11}$ circular modes in field distribution. The $TE_{10}$ and $TM_{12}$ modes have approximately the same phase. The horn radiated the $TE_{12}$ mode at the higher-frequency end of the band, which caused pattern distortion over a narrow frequency range. Both the $TM_{12}$ and $TE_{12}$ modes are excited by the electric field between the ridges. The interplay of these three modes causes rapid changes in the beam shape as frequency changes. The horn exhibits these changes at the high end of the frequency band when all three modes exist with nearly equal power. Measurements on a dual-ridged horn produced patterns that reduced to the same three dominant modes as the square quad-ridged horn radiated and produced similar results.

We fail to obtain a close match with the measured pattern of the quad-ridged horn by using the aperture currents beyond the 10-dB beamwidth for an aperture small in wavelengths. If we include currents excited along the outside of the horn bell in the physical optics analysis, we better match the measured pattern. This illustrates that the pattern of a horn is determined not only by aperture fields but also by the currents that flow down the bell. Figure 7-18 shows the measured $E$- and $H$-plane patterns and the cross-polarization in the diagonal plane. The three-dimensional measured pattern plot in Figure 7-19 at 6 GHz shows the four cross-polarization lobes in the diagonal planes.

The average pattern beamwidth matches a reflector with $f/D = 1$ and has an average illumination loss of 3 dB, with the value ranging from 2.5 to 4 dB. The average taper loss is 1.07 dB and the average spillover loss 1.08 dB. The cross-polarization exhibited in Figure 7-19 contributes an average 0.7 dB of loss. The phase-center location measurements show that the horn has up to $2\lambda$ astigmatism, which contributes 0.4 dB of loss when used as a reflector feed.

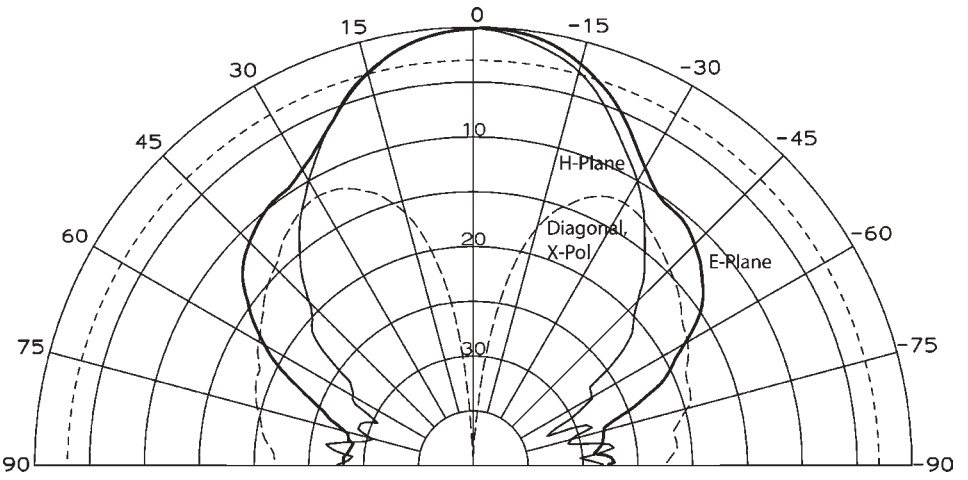


**FIGURE 7-18** Measured pattern of a circular quad-ridged horn.

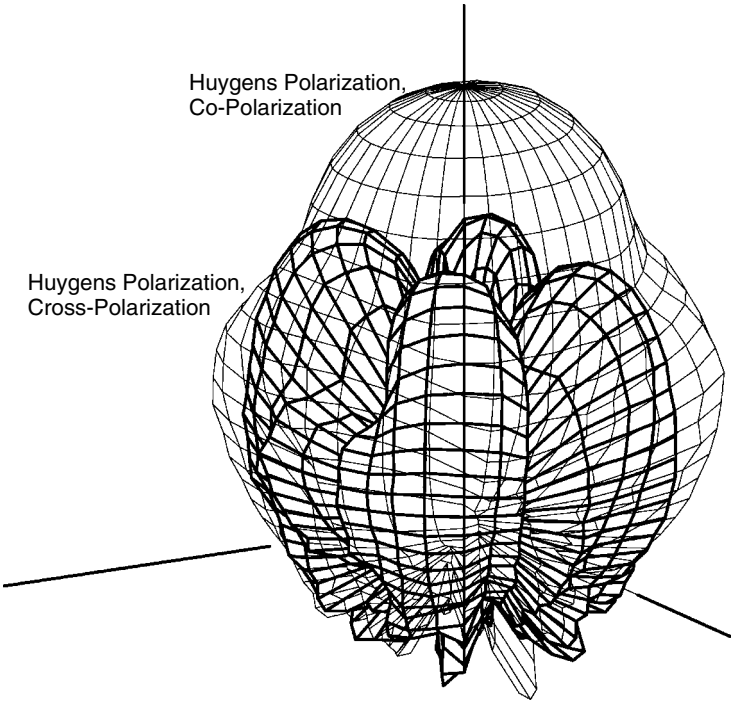


**FIGURE 7-19** Spherical radiation pattern of a circular quad-ridged horn showing four-way symmetry of cross-polarization in diagonal planes.

## 7-7 BOX HORN [32, pp. 377–380]

With a box horn (Figure 7-20), multiple waveguide modes are used to decrease the $H$-plane amplitude taper loss and axial length of the horn. We add the $TE_{30}$ mode to

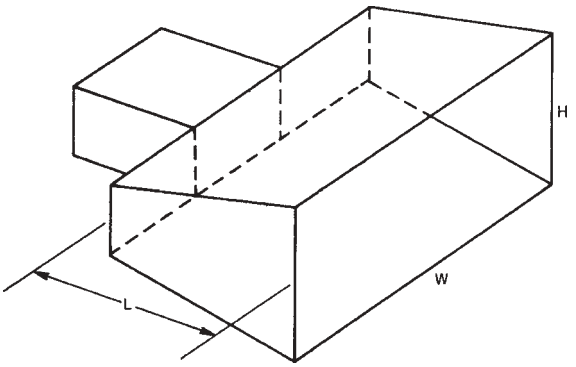


**FIGURE 7-20** Box horn.

the $TE_{10}$ mode to reduce the cosine distribution taper of the $H$-plane. By phasing the modes 180° out of phase in the center of the aperture, the $\cos 3\pi x$ distribution subtracts from the $TE_{10}$-mode distribution in the center and adds in the region near the edges.

A step in the width of a waveguide generates $TE_{N0}$ modes when fed by the $TE_{10}$ mode. Any modes not cut off by the waveguide will propagate to the aperture. If we maintain symmetry about the axis of the waveguide, only odd-order modes ($TE_{30}$, $TE_{50}$, etc.) will be generated. The width $W$ of the waveguide (Figure 7-20) beyond the step determines the possible propagating modes: $\lambda_c = 2W/N$, where $N$ is the mode number. If we limit the modes to the $TE_{10}$ and $TE_{30}$ modes in the aperture, the cutoff wavelength of the $TE_{50}$ mode determines the maximum width: $W_{\max} = 2.5\lambda$. The $TE_{30}$-mode cutoff wavelength establishes the minimum width: $W_{\min} = 1.5\lambda$. Within this range, short horns with good aperture efficiency can be designed. We can flare the $E$-plane to increase its aperture (Figure 7-20), but the limited axial length of the horn bounds the possible flare without an excessive phase error loss. The $H$-plane can also be flared, but flaring it complicates the design for the proper length $L$. The step generates smaller amplitudes of higher-order modes with each increase in $N$. Small amounts of higher-order modes ($TE_{50}$, $TE_{70}$, etc.) will decrease the efficiency only marginally, since the mode amplitudes are small.

The step generates modes in phase with the input $TE_{10}$ mode, since the higher-order modes must peak in the center and subtract from the $TE_{10}$ fields on the back wall of the larger waveguide section. The aperture distribution is a sum of $TE_{10}$ and $TE_{30}$ modes:

$$E_y(x) = a_1 \cos \frac{\pi x}{W} \exp(-jk_{10}L) + a_3 \cos \frac{3\pi x}{W} \exp(-jk_{30}L) \tag{7-46}$$

where $k_{10}$ and $k_{30}$ are the propagation constants of the two modes. The amplitude distribution in the $H$-plane will be more nearly uniform if the phase between the modes is 180°. The modes travel from the step with different phase velocities, depending on their cutoff frequencies. We adjust the length $L$ to give a 180° phase difference between the modes:

$$(k_{10} - k_{30})L = \pi$$

where $k_{10} = k\sqrt{1 - (\lambda/2\,W)^2}$ and $k_{30} = k\sqrt{1 - (3\lambda/2\,W)^2}$. We solve for the length:

$$L = \frac{\lambda/2}{\sqrt{1 - (\lambda/2\,W)^2} - \sqrt{1 - (3\lambda/2\,W)^2}} \tag{7-47}$$

**TABLE 7-10 Box Horn Characteristics**

| $TE_{30}/TE_{10}$ (Voltages) | Ratio of Input Waveguide to Aperture | Linear $ATL_w$ (dB) | $(W/\lambda)\sin\theta$ | |
|---|---|---|---|---|
| | | | 3 dB | 10 dB |
| 0.00 | 1.000 | 0.91 | 0.594 | 1.019 |
| 0.05 | 0.940 | 0.78 | 0.575 | 0.981 |
| 0.10 | 0.888 | 0.67 | 0.558 | 0.947 |
| 0.15 | 0.841 | 0.58 | 0.544 | 0.917 |
| 0.20 | 0.798 | 0.52 | 0.530 | 0.890 |
| 0.25 | 0.758 | 0.48 | 0.518 | 0.866 |
| 0.30 | 0.719 | 0.46 | 0.507 | 0.844 |
| 0.35 | 0.682 | 0.46 | 0.496 | 0.824 |
| 0.40 | 0.645 | 0.47 | 0.487 | 0.806 |
| 0.45 | 0.609 | 0.50 | 0.479 | 0.790 |
| 0.50 | 0.573 | 0.54 | 0.471 | 0.775 |
| 0.55 | 0.537 | 0.60 | 0.463 | 0.761 |
| 0.60 | 0.500 | 0.66 | 0.456 | 0.749 |
| 0.65 | 0.462 | 0.74 | 0.450 | 0.737 |
| 0.70 | 0.424 | 0.82 | 0.444 | 0.726 |

The ratio of the modes generated by the step can be found from mode matching on the input waveguide aperture of width $a$:

$$\frac{a_N}{a_1} = \frac{\displaystyle\int_{-a/2}^{a/2} \cos(\pi x/a)\cos(N\pi x/W)dx}{\displaystyle\int_{-a/2}^{a/2} \cos(\pi x/a)\cos(\pi x/W)dx} \tag{7-48}$$

where $a_N$ is the $TE_{N0}$ mode amplitude. Table 7-10 lists the step dimensions needed to design to a given ratio of modes. The amplitude taper loss is a minimum at $a_3/a_1 = 0.32$. The possible 3-dB beamwidths with a single mode, $TE_{10}$, range from 20 to 44°.

***Example*** Design a box horn with an $H$-plane 10-dB beamwidth of 50°.

We pick $a_3/a_1 = 0.35$. From Table 7-10, $(W/\lambda)\sin\theta = 0.824$. The obliquity factor at 25° adds 0.42 dB of loss. We must design with a wider 10-dB beamwidth. This is within the permissible range for only two modes in the aperture. We calculate the length to phase the modes by 180° by using Eq. (7-47): $L = 1.451\lambda$. The horn is shorter than the aperture width.

## 7-8 T-BAR-FED SLOT ANTENNA

A T-bar-fed slot antenna (Figure 7-21) looks more like an open-circuited waveguide to coax transition than a slot. Like a slot, its pattern is very broad. The antenna has been designed experimentally [33, pp. 184–190] and those dimensions provide a good starting point. Table 7-11 lists two designs [33] referred to Figure 7-21. The aperture admittance is a combination of the radiation admittance and a capacitive

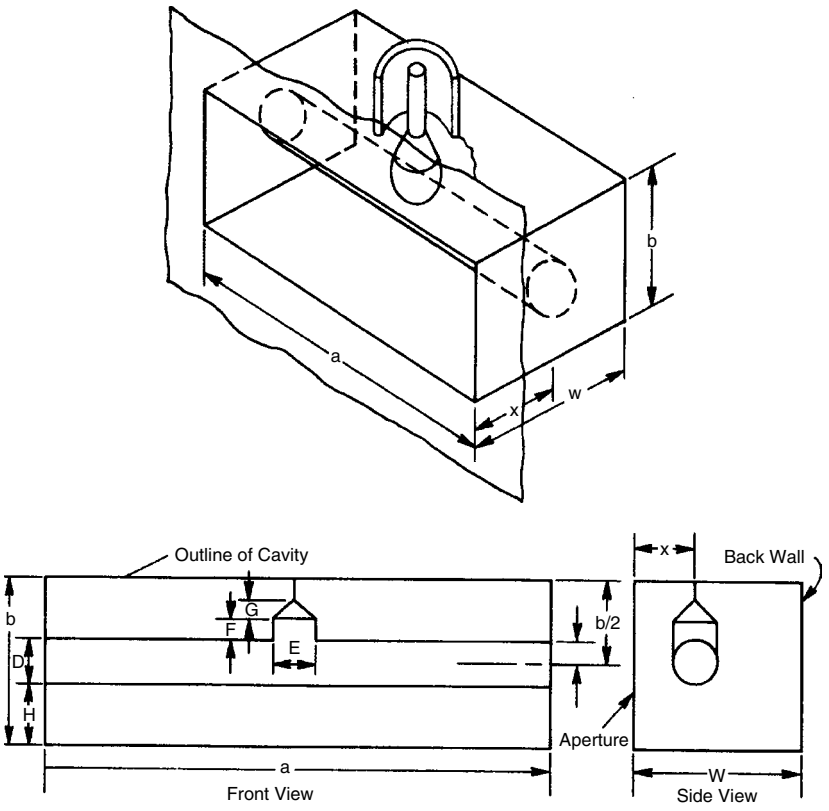


**FIGURE 7-21** T-bar-fed cavity slot antenna. (From [34], © 1975 IEEE.)

**TABLE 7-11 Dimensions for Two Antenna Designs**

| Dimensions | Antenna 1 | Antenna 2 |
|---|---|---|
| *b/a* | 0.323 | 0.226 |
| *W/a* | 0.323 | 0.295 |
| *x/a* | 0.118 | 0.113 |
| *D/a* | 0.118 | 0.090 |
| *I/a* | 0.059 | 0.045 |
| *E/a* | 0.118 | 0.090 |
| *F/a* | 0.057 | 0.045 |

susceptance. Behind the feed point, the length of short-circuited waveguide adds an inductive susceptance that grows as frequency decreases. The horizontal bar produces a capacitive susceptance at the input to counteract the back-wall susceptance. These susceptances track with frequency changes; each one decreases to maintain the sum near resonance.

Later experimental work [34] revealed further properties of the antenna. Measurements on antenna 1 show that the lower-end 2 : 1 VSWR band edge occurs when $a = 0.57\lambda$ and the upper end when $a = 0.9\lambda$. The bandwidth is about 1.6 : 1.

Antenna 2 was reported [33] as having less bandwidth than antenna 1. When the round rod was replaced with a flat strip, whose width across the guide was the same as the diameter of the rod, almost identical results were obtained. We have a choice. The flat strip is an easier construction, but the round rod gives better mechanical support in all axes to withstand shock and vibration.

The flat strip adds to the freedom of design. The bandwidth potential increases when $H$ is decreased while $I$ is held constant. Newman and Thiele [34] found that when $H$ was decreased, the nominal impedance level was raised. When the input impedance is plotted on the Smith chart, the locus is centered about a higher resistance. By adding a broadband impedance transformer on the input, we can achieve the higher bandwidth potential. Newman and Thiele achieved a nearly 2 : 1 VSWR bandwidth from $a = 0.52\lambda$ to $a = 1.12\lambda$, or 2.3 : 1 bandwidth.

## 7-9 MULTIMODE CIRCULAR HORN [35]

A step in the diameter of a circular waveguide generates a $TM_{11}$ mode to satisfy the boundary conditions. The fields of the $TM_{11}$ mode can be phased to cancel the fields from the $TE_{11}$ mode at the edges of the aperture in the $E$-plane. The tapering of the fields in the aperture reduces the $E$-plane sidelobes while broadening the beamwidth. Equalizing the field distributions in the two planes helps to bring the $E$- and $H$-plane phase centers closer together.

The modes generated by the step are more complicated than those for the box horn. Symmetry eliminates generation of the unwanted modes: $TM_{01}$, $TE_{21}$, and $TE_{01}$. The step transition shifts the phase of the $TM_{11}$ mode relative to the $TE_{11}$ mode [36]. Since the waveguide modes have different phase velocities, they can be phased to produce the desired field at the aperture. Although calculated information [36] is helpful, the designs must be completed empirically. The required phasing to achieve field cancellation limits the bandwidth, but for narrowband applications a stepped horn is cheaper than a corrugated horn.

Satoh [37] loads the flare of a conical horn with a conical dielectric step to generate the $TM_{11}$ mode. Symmetry prevents the excitation of unwanted modes. He places the step at a diameter where the $TM_{11}$ mode can propagate. By using two steps, the bandwidth can be increased because the lengths can be adjusted to give perfect mode cancellation at two frequencies. We can replace the dielectric cone by metal steps each of which generates the $TM_{11}$ mode and thereby achieve good results, in theory, at multiple frequencies.

## 7-10 BICONICAL HORN [4]

A biconical horn consists of two cones with a common vertex. The angle of the generating lines of the cones is measured from a common axis. The cones of the usual antenna have angles that sum to 180°. Spherical modes describe the fields between the cones, but we can use approximations with good results. The lowest-order mode is TEM between the cones and is easily excited by a coax line. The outer conductor connects to one cone, and the second cone feeds out of the center conductor. The electric field of the TEM mode is polarized in the direction of the axis. The first higher-order mode

has a circulating electric field with the magnetic field in the direction of the axis. It can be excited either from a $TE_{01}$-mode circular waveguide or by an array of slots on a cylinder. The distance between cones must be at least $\lambda/2$ at the point of excitation of the $TE_{01}$ biconical mode.

We approximate the distribution of the zeroth-order mode, TEM, as uniform along the axis. The first-order mode, $TE_{01}$, distribution is approximately cosine along the axis. We calculate gain by using aperture distribution losses. We describe the horn with a slant radius along the generating line and a height between the ends of the cones. The expansion in spherical modes requires integration over a spherical cap at the aperture if a constant phase surface is used. We obtain good results by using a cylindrical aperture and a quadratic phase distribution. The antenna has circular symmetry about the $z$-axis that bounds the directivity to $2L/\lambda$. We use linear distribution efficiencies to compute directivity (gain):

$$\text{gain} = 10 \log \frac{2L}{\lambda} - \text{ATL}_x - \text{PEL}_x \tag{7-49}$$

The TEM mode has a uniform distribution, so we use the "uniform" column of Table 4-42 to calculate phase error loss. The uniform distribution has no amplitude taper loss. The cosine distribution of the first-order mode requires an ATL = 0.91 dB and use of the cosine distribution quadratic phase error loss of Table 4-42. Given the height between the ends of the cones, $H$, and the slant radius $R$, we determine the quadratic phase distribution constant from

$$S = \frac{H^2}{8\lambda R} \tag{7-50}$$

***Example*** Compute the gain of a biconical horn with a slant radius of $10\lambda$ and cone angles of $75^\circ$ and $105^\circ$. $H = 2R \cos 75^\circ = 5.176\lambda$ and $S = 0.33$.

From Table 4-42, we read

$$\text{PEL}_{\text{TEM}} = -1.76\,\text{dB} \quad \text{PEL}_{\text{TE}-01} = -0.79\,\text{dB}$$

Vertical mode, TEM: gain $= 10 \log[2(5.176)] + \text{PEL}_{\text{TEM}}$:

$$10.15\,\text{dB} - 1.76\,\text{dB} = 8.4\,\text{dB}$$

Horizontal mode, $TE_{01}$: gain $= 10 \log[2(5.176)] + \text{PEL}_{\text{TE}-01} + \text{ATL}_{\text{cosine}}$:

$$10.15\,\text{dB} - 0.79\,\text{dB} - 0.91\,\text{dB} = 8.45\,\text{dB}$$

We can calculate beamwidths by using the results of the rectangular horn, where we measure the angles from $\theta = 90^\circ$ for the complementary-angled biconical horn.

***Example*** Compute the 3-dB beamwidths of the horn above. $S = 0.33$ and $H = 5.176\lambda$.

Use Table 7-2 with the TEM mode and $\alpha$ as the angle from $\theta = 90^\circ$:

$$\frac{H}{\lambda} \sin \alpha = 0.5015 \quad \alpha = 5.56^\circ$$

The obliquity factor is insignificant.

$$\text{HPBW} = 11.1^\circ \qquad \text{TEM mode}$$

Use Table 7-1 with the $TE_{01}$ mode.

$$\frac{H}{\lambda}\sin\alpha = 0.6574 \qquad \text{HPBW} = 14.6^\circ \qquad TE_{01} \text{ mode}$$

The two modes have about the same gain, but the $TE_{01}$ mode has a greater beamwidth. When we refer to Figures 7-3 and 7-4, we see that the TEM-mode horn has about 7-dB sidelobes and the $TE_{01}$-mode horn has practically no sidelobes. The sidelobes reduce the gain of the TEM mode with its narrower beamwidth.

## REFERENCES


1. A. W. Love, ed., *Electromagnetic Horn Antennas*, IEEE Press, New York, 1976.
2. W. L. Barrow and L. J. Chu, Theory of electromagnetic horn, *Proceedings of IRE*, vol. 27, January 1939, pp. 51–64.
3. M. C. Schorr and E. J. Beck, Electromagnetic field of the conical horn, *Journal of Applied Physics*, vol. 21, August 1950, pp. 795–801.
4. S. A. Schelkunoff and H. Friis, *Antenna Theory and Practice*, Wiley, New York, 1952.
5. P. M. Russo et al., A method of computing $E$-plane patterns of horn antennas, *IEEE Transactions on Antennas and Propagation*, vol. AP-13, no. 2, March 1965, pp. 219–224.
6. J. Boersma, Computation of Fresnel integrals, *Mathematics of Computation*, vol. 14, 1960, p. 380.
7. K. S. Kelleher, in H. Jasik, ed., *Antenna Engineering Handbook*, McGraw-Hill, New York, 1961.
8. D. G. Bodnar, Materials and design data, Chapter 46 in R. C. Johnson, ed., *Antenna Engineering Handbook*, 3rd ed., McGraw-Hill, New York, 1993.
9. E. H. Braun, Gain of electromagnetic horns, *Proceedings of IRE*, vol. 41, January 1953, pp. 109–115.
10. E. I. Muehldorf, The phase center of horn antennas, *IEEE Transactions on Antennas and Propagation*, vol. AP-18, no. 6, November 1970, pp. 753–760.
11. A. J. Simmons and A. F. Kay, The scalar feed: a high performance feed for large paraboloid reflectors, Design and Construction of Large Steerable Aerials, *IEE Conference Publication* 21, 1966, pp. 213–217.
12. B. M. Thomas, Design of corrugated conical horns, *IEEE Transactions on Antennas and Propagation*, vol. AP-26, no. 2, March 1978, pp. 367–372.
13. T. S. Chu and W. E. Legg, Gain of corrugated conical horn, *IEEE Transactions on Antennas and Propagation*, vol. AP-30, no. 4, July 1982, pp. 698–703.
14. G. L. James, $TE_{11}$ to $HE_{11}$ mode converters for small angle corrugated horns, *IEEE Transactions on Antennas and Propagation*, vol. AP-30, no. 6, November 1982, pp. 1057–1062.
15. P. J. B. Clarricoats and P. K. Saha, Propagation and radiation of corrugated feeds, *Proceedings of IEE*, vol. 118, September 1971, pp. 1167–1176.
16. A. W. Rudge et al., eds., *The Handbook of Antenna Design*, Vol. 1, Peter Peregrinus, London, 1982.

17. G. L. James and B. M. Thomas, $TE_{11}$-to-$HE_{11}$ corrugated cylindrical waveguide mode converters using ring-loaded slots, *IEEE Transactions on Microwave Theory and Techniques*, vol. MTT-30, no. 3, March 1982, pp. 278–285.
18. R. Wohlleben, H. Mattes, and O. Lochner, Simple small primary feed for large opening angles and high aperture efficiency, *Electronics Letters*, vol. 8, September 21, 1972, pp. 474–476.
19. A. D. Olver et al., *Microwave Horns and Feeds*, IEEE Press, New York, 1994.
20. G. L. James, Radiation properties of 90° conical horns, *Electronics Letters*, vol. 13, no. 10, May 12, 1977, pp. 293–294.
21. A. Kumer, Reduce cross-polarization in reflector-type antennas, *Microwaves*, March 1978, pp. 48–51.
22. P.-S. Kildal, *Foundations of Antennas*, Studentlitteratur, Lund, Sweden, 2000.
23. S. Maci et al., Diffraction at artificially soft and hard edges by using incremental theory of diffraction, *IEEE Antennas and Propagation Symposium*, 1994, pp. 1464–1467.
24. B. A. Saleh and M. C. Teich, *Fundamentals of Photonics*, Wiley, New York, 1991.
25. K. Pontoppidan, ed., *Technical Description of Grasp 8*, Ticra, Copenhagen, 2000 (self published and available at www.ticra.com).
26. P. F. Goldsmith, *Quasioptical Systems*, IEEE Press, New York, 1998.
27. L. Diaz and T. A. Milligan, *Antenna Engineering Using Physical Optics*, Artech House, Boston, 1996.
28. J. L. Kerr, Short axial length broadband horns, *IEEE Transactions on Antennas and Propagation*, vol. AP-21, no. 5, September 1973, pp. 710–714.
29. J. R. Whinnery and H. W. Jamieson, Equivalent circuits for discontinuities in transmission lines, *Proceedings of IRE*, vol. 32, no. 2, February 1944, pp. 98–114.
30. S. B. Cohn, Properties of ridge waveguide, *Proceedings of IRE*, vol. 35, no. 8, August 1947, pp. 783–788.
31. M. H. Chen, G. N. Tsandoulas, and F. W. Willwerth, Modal characteristics of quadruple-ridged circular and square waveguide, *IEEE Transactions on Microwave Theory and Techniques*, vol. MTT-21, August 1974, pp. 801–804.
32. S. Silver, ed., *Microwave Antenna Theory and Design*, McGraw-Hill, New York, 1949.
33. A. Dome and D. Lazarno, Radio Research Laboratory Staff, *Very High Frequency Techniques*, McGraw-Hill, New York, 1947, pp. 184–190.
34. E. H. Newman and G. A. Thiele, Some important parameters in the design of T-bar fed slot antennas, *IEEE Transactions on Antennas and Propagation*, vol. AP-23, no. 1, January 1975, pp. 97–100.
35. P. D. Potter, A new horn antenna with suppressed sidelobes and equal beamwidths, *Microwaves*, vol. 6, June 1963, pp. 71–78.
36. W. J. English, The circular waveguide step-discontinuity mode transducer, *IEEE Transactions on Microwave Theory and Techniques*, vol. MTT-21, no. 10, October 1973, pp. 633–636.
37. T. Satoh, Dielectric loaded horn antenna, *IEEE Transactions on Antennas and Propagation*, vol. AP-20, no. 2, March 1972, pp. 199–201.